AD-766 331

MAGNETIC RARE EARTH COMPOUNDS III

HEWLETT-PACKARD CO.

PREPARED FOR
ADVANCED RESEARCH PROJECTS AGENCY

JULY 1973

MAGNETIC RARE EARTH COMPOUNDS III

Hewlett-Packard Company

Palo Alto, California 94304

FINAL TECHNICAL REPORT

JULY 1973

Contract No. DAAH01-72-C-0996
Program Code No. OD10

ARPA Support Office
Research, Development, Engineering,
and Missile Systems Laboratory
U.S. Army Missile Command
Redstone Arsenal, Alabama

A Research Project Sponsored by the Advanced Research Projects Agency, Department of Defense, Washington, D.C., ARPA Order 1627

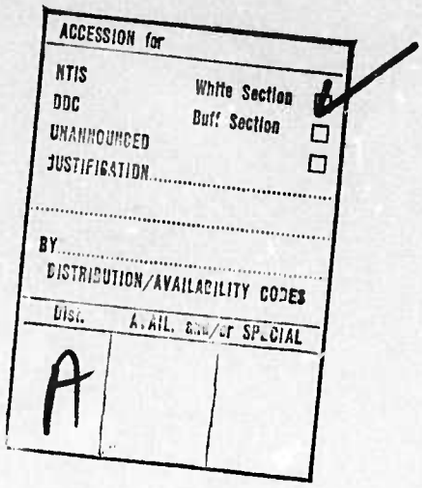

NOTICE

"This research was sponsored by the Advanced Research Projects Agency of the Department of Defense under ARPA Order 1627 and was monitored by the U.S. Army Missile Command under Contract Number DAAH01-72-C-0996. Views and conclusions expressed herein are the primary responsibility of the author or the contractor and should not be interpreted as representing the official opinion or policy of USAMICOM, ARPA, DOD or any other agency of the Government."

Unclassified
Security Classification

DOCUMENT CONTROL DATA - R&D
(Security classification of title, body of abstract and indexing annotation must be entered when the overall report is classified)

1 ORIGINATING ACTIVITY (Corporate author)
Hewlett-Packard Company
1501 Page Mill Road
Palo Alto, California 94304

2a. REPORT SECURITY CLASSIFICATION
Unclassified

2b GROUP

3 REPORT TITLE
MAGNETIC RARE EARTH COMPOUNDS III

4 DESCRIPTIVE NOTES (Type of report and inclusive dates)
Final Technical Report (June 14, 1972 to June 14, 1973)

5 AUTHOR(S) (Last name, first name, initial)
Ronald Hiskes

6 REPORT DATE	7a. TOTAL NO. OF PAGES	7b. NO. OF REFS
July 1973	~~80~~ 80	26

8a. CONTRACT OR GRANT NO.	9a. ORIGINATOR'S REPORT NUMBER(S)
DAAH01-72-C-0996	
b. PROJECT NO. Technical Requirement No. 1335	
c. Program Code No. 0D10	9b. OTHER REPORT NO(S) (Any other numbers that may be assigned this report)
d. ARPA Order No. 1627	

10. DISTRIBUTION STATEMENT
Approved for public release; distribution unlimited.

11. SUPPLEMENTARY NOTES	12. SPONSORING MILITARY ACTIVITY
	Advanced Research Projects Agency Department of Defense, Washington, D.C., ARPA Order 1627

13. ABSTRACT

The magnetically uniaxial rare earth iron garnet $(Sm,Y)_3(Ga,Fe)_5O_{12}$ has been grown on {111} $Gd_3Ga_5O_{12}$ substrates. The liquid phase epitaxial dipping technique with horizontal substrate rotation has been employed in conjunction with $PbO-B_2O_3$ and $BaO-B_2O_3-BaF_2$ solvents in the temperature range of 900°C-1030°C.

Growth parameters in both solvents, such as growth temperature, supercooling, and rotation rate, have been correlated with changes in growth rate and properties of the films. The distribution coefficient of gallium has been found to be relatively insensitive to growth rate in the BaO-based solvent, in contrast to the PbO-based solvent.

The films have been characterized with respect to composition, impurity content, lattice parameter, optical properties and magnetic properties. Films of similar composition grown in each solvent have comparable magnetic properties, but the optical absorption coefficient, lattice parameter and impurity content are higher in the epitaxial layers grown in the $PbO-B_2O_3$ solvent.

i

DD FORM 1 NOV 68 1473 REPLACES DD FORM 1473, 1 JAN 64, WHICH IS OBSOLETE FOR ARMY USE.

Unclassified
Security Classification

14. KEY WORDS	LINK A		LINK B		LINK C	
	ROLE	WT	ROLE	WT	ROLE	WT
Garnets						
Rare Earths						
Magnetic Bubbles						
Liquid Phase Epitaxy						
BaO-based Solvents						
Crystal Growth						

TECHNICAL REQUIREMENT NO. 1335
ARPA Order 1627

MAGNETIC RARE EARTH COMPOUNDS III

FINAL TECHNICAL REPORT

JULY 1973

HEWLETT-PACKARD COMPANY
Palo Alto, California 94304
(415) 493-1501

Contract No. DAAH01-72-C-0996
Program Code No. 0D10

Monitored By

ARPA Support Office
Research, Development, Engineering, and
Missile Systems Laboratory
U.S. Army Missile Command
Redstone Arsenal, Alabama

Approved for Public Release
Distribution Unlimited

A Research Project Sponsored by the Advanced
Research Projects Agency, Department of
Defense, Washington, D.C., ARPA Order 1627

FOREWORD

This report describes work performed under Contract DAAH01-72-C-0996 for the ARPA Support Office, Research, Development, and Missile Systems Laboratory, U.S. Army Missile Command, Redstone Arsenal, Alabama, during the period June 14, 1972 through June 14, 1973. The monitors for this project were J. Shelton and R. Norman. The work was performed in the Solid-State Laboratory of Hewlett-Packard Laboratories under the direction of P. E. Greene. The work was supervised by R. A. Burmeister, and this report was written by R. Hiskes.

The author gratefully acknowledges the assistance of R. B. Clover, L. Cutler, R. L. Lacey and R. Waites with the magnetic characterization of films. T. L. Felmlee polished the substrates and performed the optical absorption and lattice parameter measurements. F. Perlaki and L. Small helped design, construct and operate the crystal growth apparatus.

SUMMARY

The magnetically uniaxial rare earth iron garnet $(Sm,Y)_3(Ga,Fe)_5O_{12}$ has been grown on {111} $Gd_3Ga_5O_{12}$ substrates. The liquid phase epitaxial dipping technique with horizontal substrate rotation has been employed in conjunction with $PbO-B_2O_3$ and $BaO-B_2O_3-BaF_2$ solvents in the temperature range of 900°C-1030°C.

Growth parameters in both solvents, such as growth temperature, supercooling, and rotation rate, have been correlated with changes in growth rate and properties of the films. The distribution coefficient of gallium has been found to be relatively insensitive to growth rate in the BaO-based solvent, in contrast to the PbO-based solvent.

The films have been characterized with respect to composition, impurity content, lattice parameter, optical properties and magnetic properties. Films of similar composition grown in each solvent have comparable magnetic properties, but the optical absorption coefficient, lattice parameter and impurity content are higher in the epitaxial layers grown in the $PbO-B_2O_3$ solvent.

TABLE OF CONTENTS

TABLE OF CONTENTS

(Continued)

LIST OF ILLUSTRATIONS

LIST OF ILLUSTRATIONS

(Continued)

LIST OF ILLUSTRATIONS

(Continued)

LIST OF ILLUSTRATIONS

(Continued)

LIST OF TABLES

SECTION I

1.0 SUMMARY

1.1 Program Plan and Objective

The potential of magnetically uniaxial rare earth compounds for magnetic bubble memory devices led to the initiation of a materials program at Hewlett-Packard Laboratories (HPL) to investigate the preparation and properties of these compounds. The first material studied was $YFeO_3$, which required thin single crystalline films of c-axis orientation approximately 75 μm thick to stabilize the bubble domains. Since $YFeO_3$ loses oxygen readily in air at its melting point of 1680°C[1], the most direct method of materials preparation was bulk solution growth of single crystals, followed by slicing and polishing to the desired thickness.

The commonly used PbO-based solvent has a number of significant disadvantages, and therefore, a new solvent system was invented for the growth of $YFeO_3$ and the rare earth orthoferrites, comprised of BaO, B_2O_3 and BaF_2. This solvent, patterned after the $BaO-B_2O_3$ solvent first used by Linares in 1962 for the growth of $Y_3Fe_5O_{12}$[2], was developed and high quality crystals of $YFeO_3$ exhibiting magnetic bubble domains were grown in it.

In 1970, the discovery of uniaxial magnetic anisotropy in the rare earth iron garnets was announced by Bell Laboratories[3], which promised significant advantages compared to the orthoferrites. The most important of these advantages were smaller bubble size resulting in an order of magnitude greater packing density, and the feasibility of epitaxial growth on paramagnetic garnet substrates to eliminate the slicing and

polishing operations necessary to produce the requisite thin film of active material. The direction of the HPL bubble program now shifted to the liquid phase epitaxial (LPE) growth of the magnetically uniaxial garnets, and it was decided to develop the techniques of LPE growth in both the PbO-based and the BaO-based solvents in order to directly compare the relative merits of each. This approach has advanced the state-of-the-art of bubble materials technology as will be demonstrated in the body of this report.

The specific objectives of the bubble program at HPL were as follows:

1. Development of practical techniques for the growth of single crystals of rare earth compounds having properties suitable for studies and utilization of bubble domain phenomena.
2. Acquisition of the necessary data to better characterize and quantitatively describe both the crystal growth process and the salient physical and chemical properties of the crystals produced.
3. Determination of the relationship between methods and parameters of the crystal growth process and relevant physical properties of the crystals thus grown.

1.2 Accomplishments

The most important specific accomplishments of the HPL magnetic bubble program are as follows:

1. During the first year of the contract, the bulk growth of

$YFeO_3$ was successfully demonstrated in the BaO-based solvent, and defect free films 75 μm thick and up to 3 x 3 mm in cross section were produced by appropriate slicing and polishing techniques. The $YFeO_3$ was grown by both a slow cooling solution technique and by a unique thermal gradient steady state method[4]. Using the steady state (isothermal growth interface) technique, $YFeO_3$ was also grown homoepitaxially on a $YFeO_3$ seed. Epitaxial layers grown by this technique contained fewer bubble pinning defects than the substrates upon which they were grown. Heteroepitaxy of $YFeO_3$ on $YAlO_3$ was also attempted, but the rapid attack of the $YAlO_3$ substrate by the BaO-based solvent precluded successful heteroepitaxial growth. Similar results were subsequently reported for the conventional PbO-based solvent[5]. Domain wall mobility in the $YFeO_3$ grown in the BaO-based solvent exceeded 4000 cm/sec-Oe, comparable to the best $YFeO_3$ grown from the PbO-based solvent[6].

2. During the second year of the contract, materials emphasis shifted to the technologically more interesting rare earth iron garnets, and thin films of $(Eu,Er)_3(Fe,Ga)_5O_{12}$ and $(Gd,Y,Yb)_3(Fe,Ga)_5O_{12}$ were grown by vertical dipping and horizontal rotation LPE techniques on $Gd_3Ga_5O_{12}$ substrates[7]. These films exhibited domain wall mobilities ranging from 80 cm/sec-Oe for the (Eu,Er) compositions to greater than 2000 cm/sec-Oe for the (Gd,Y,Yb) compositions.

3. In the final year of the contract, a very high degree of control over the growth process was achieved, using the $(Gd,Y,Yb)_3(Fe,Ga)_5O_{12}$ composition as a vehicle. Since this composition suffered from high temperature sensitivity, attention shifted to the composition $(Sm,Y)_3(Fe,Ga)_5O_{12}$, which appeared to satisfy all the magnetic bubble device requirements. These

requirements for a particular set of specifications are listed in Table I. The high degree of control over the growth process was confirmed by the fact that device quality films meeting all the materials specifications in Table I were being routinely grown in the BaO-based solvent within 10 days after the initial growth run.

4. The $BaO-B_2O_3-BaF_2$ solvent has been characterized with respect to the liquidus surface as a function of composition, density, solubility of $YFeO_3$ and the garnets as a function of temperature, and the stability range for the orthoferrite and garnet phases. This work has been of necessity very limited, and while the optimum growth conditions may not have yet been found, adequate conditions have been discovered and thoroughly tested.

5. The growth process has been characterized in both the $PbO-B_2O_3$ solvent and the $BaO-B_2O_3-BaF_2$ solvent with respect to supersaturation and fluid motion effects upon growth rate, thickness uniformity and defect generation in the garnet films. Thickness has been measured as a function of growth time, and defects in the garnet films have been studied as a function of the solute composition.

6. Substrate preparation techniques have been developed which permit reproducible production of $Gd_3Ga_5O_{12}$ substrates having less than 5 defects (scratches, particulate matter) per cm^2.

7. Garnet film and substrate characterization techniques have been developed to measure film composition and perfection, lattice parameter mismatch, impurity content, and magnetic properties including magnetization, anisotropy, characteristic length, collapse field, wall energy, Néel temperature, mobility and coercivity, and the temperature dependence of the magnetic properties.

TABLE I

Specifications and Accomplishments for Magnetic Bubble Materials

Material Property	Specifications (established 3/72)	Recent Values for $Sm_{.35}Y_{2.65}Ga_{1.2}Fe_{3.8}O_{12}$	Related Oevice Operating Characteristic
Film Thickness Run-to-Run Variation Variation Over the Surface	3.5 μm ±5% ±1%	3.5 μm ±5% ±1%	Bit Size Bit Oensity
Bubble Oiameter	6 μm	6 μm	
Bubble Ellipticity	< 0.2	< 0.2	
Characteristic Length Run-to-Run Variation Variation Over the Surface	0.8 μm ±5% ±1%	0.8 μm ±5% ±1%	A Compromise Between Drive Field, Power Requirements, Ease of Oetection, and Bubble Size and Stability
Saturation Magnetization Run-to-Run Variation Variation Over the Surface	75 - 150 Gauss ±5% ±1%	130 Gauss ±5% ±1%	
Anisotropy Field	> 2 · Magnetization	6 · Magnetization	
Mobility	> 200 cm/Oe-sec	280 cm/Oe-sec	Oata Rate
Coercive Force	< 0.3 Oe	0.3 Oe	
Temperature Coefficient of Characteristic Length	< 0.001 μm/°K	0.004 μm/°K	Operating Stability over > 50°C Temperature Range
Density of Crystal Defects Which Affect Magnetic Properties	< $5/cm^2$	< $5/cm^2$	High Yield of Bubble Chips
Usable Defect Free Area	> 1 mm^2	> 50 mm^2	

8. Reproducibility experiments have been carried out in both the PbO-based and BaO-based solvents to determine the degree of process control required to maintain the film properties within desired limits over long periods of time and for many subsequent growth runs.

9. The growth process and properties of the films grown in each solvent system have been compared to determine the relative merits and deficiencies of each, both as an aid to a better understanding of the growth process itself and as a means for optimizing the process. In order to compare impurity incorporation and its effect on lattice parameter, for example, films of $Y_3Fe_5O_{12}$ (in which the composition is fixed) have been grown in the PbO-based and the BaO-based solvents at the same temperature in order to directly compare their magnetic and optical properties.

1.3 Publications and Patents

The work performed during the course of this contract resulted in the following contributions to the scientific literature.

1. R. Hiskes, T. L. Felmlee and R. A. Burmeister, "Growth of Rare Earth Orthoferrites and Garnets Using BaO-Based Solvents," Journal of Electronic Materials 1, 458 (1972).

2. R. Hiskes, "Materials for Magnetic Bubble Devices," Western Electronics Show and Convention (WESCON) Proceedings, Technical Session No. 8, September, 1972.

3. R. Hiskes and R. A. Burmeister, "Properties of Rare Earth Iron Garnets Grown in BaO-Based and PbO-Based Solvents," AIP Conference Proceedings, No. 10, Part 1, p. 304, 18th Annual Conference on Magnetism and Magnetic Materials, Denver, 1972.

4. R. Hiskes, "Method and Flux for Growing Single Crystals," U.S. Patent No. 3,697,320, October 10, 1972.

SECTION II

2.0 MATERIALS PREPARATION

2.1 Historical Development

Although magnetic bubbles had been observed in uniaxial magnetic oxides as early as 1958, their potential as memory storage devices was first realized by Bobeck in 1967[8]. The first materials efforts resulted in bulk solution grown $YFeO_3$ and mixed rare earth orthoferrites with bubble diameters of 25-75 μm. Recognizing the need for smaller bubble sizes to realize higher packing densities, attempts were made to grow the hexagonal ferrites[9], which indeed exhibited bubble diameters less than 1 μm, but unfortunately were found to have disappointingly small mobilities. Then, magnetic uniaxiality was discovered in bulk and epitaxially grown rare earth iron garnets[3], which exhibited stable bubble diameters of 0.5-10 μm with mobilities exceeding 2000 cm/sec-Oe. Extensive research and development with the garnet materials has resulted in the first prototypes for bubble mass memories[10]. More recently, exploratory work with thin films of amorphous Gd-Co and Gd-Fe alloys[11] indicates uniaxial magnetic behavior in these materials as well, and the economic advantages of these films may result in their use in future generations of devices.

2.2 Preparation of Garnet Thin Films

Although the first bubble garnets were grown by bulk slow cooling solution techniques, followed by slicing and polishing to the desired orientation and thickness, the most successful method of growth has proved

to be {111} heteroepitaxial growth on a paramagnetic $Gd_3Ga_5O_{12}$ substrate. The two epitaxial techniques pursued most extensively have been vapor phase epitaxy (VPE)[12], or chemical vapor deposition (CVD), and liquid phase epitaxy (LPE). The CVD films are grown at ∿1200°C, higher than the annealing temperature required for eliminating growth induced cation ordering[13]; and, therefore, these films exhibit only stress induced anisotropy. It has also proved difficult in practice to grow films with low defect densities ($<50/cm^2$) by the CVD process, although there appears to be no fundamental reason for this. Nearly all of the bubble garnet films are now grown by well developed LPE techniques.

2.3 Control of the LPE Process

Proper control and reproducibility of the LPE process entails rigid control of the macroscopic system variables. The most important of these are the solid/liquid interface temperature and the solute boundary layer thickness, which govern the diffusion controlled solution growth process. The boundary layer depends upon the nature of fluid motion past the growth interface, which in turn is a complex function of both thermally and mechanically induced motion of the fluid, either by stirring or substrate/crucible rotation. Thermally induced convection is present whenever the top of the solution exceeds the temperature of the bottom by a critical margin, or whenever there exists a horizontal temperature gradient in the solution[14]. This type of convection can be eliminated by making the solution completely isothermal, but this is very difficult in practice for solution volumes of 20-150 cc at the crystal growth temperatures of

850-1050°C. The vertical temperature gradient can be controlled in the conventional LPE vertical dipping furnaces, but the solution is generally heated by a furnace winding around the periphery of the crucible, resulting in a small (1-3 °C/cm) radial thermal gradient. This gradient causes the fluid to rise at the sides of the crucible and descend in the central region. Perturbation of this flow by a substrate produces whorls and eddies in the solution adjacent to the substrate resulting in an unpredictable and unmanageable boundary layer thickness along the surface of the substrate. The convection currents caused by radial thermal gradients are so severe that they have been found to cause a thickness variation in a vertically grown film of up to 1 μm/cm in a 4 μm thick film (thicker at the top) even though there is a vertical temperature gradient such to make the top of the substrate 10°C hotter than the bottom.

There are two ways to reduce the convection caused by the radial gradient, the first being merely to reduce the cell size for convection by dipping a large number of vertically suspended substrates into the solution at once with a very small spacing between them. This procedure may eventually prove to be the best way to achieve economical multiple substrate growth, since with a properly designed rectangular crucible, up to 25 films can be grown at a time in a standard 4 inch bore tubular growth furnace.

The second widely used technique utilizes controllable mechanically induced convection to overcome the thermal convection, which can be achieved by rotating a horizontally held substrate[15]. The horizontal rotation (at rates of 30-500 rpm) induces a fluid flow pattern, which has been shown both theoretically and experimentally to produce a boundary layer of constant thickness over the entire area of the substrate, except at the periphery,

where edge effects dominate because of the larger diffusion volume[15-17]. This techniques does not lend itself well to multiple substrate growth, although some attempts have been made[18].

Temperature control at the interface is also critical, since differences in temperature as small as 1°C have been shown to result in large differences in growth rate and magnetic properties, largely due to the variation of distribution coefficients of the cations with temperature[15]. This control has been achieved by supercooling the garnet solution to the desired degree of supersaturation (5-30°C), and then holding at this furnace control setting until the solution has reached equilibrium temperature before inserting the substrate. The relatively short growth time of 1-20 minutes aids in maintaining temperature uniformity during growth.

2.4 Garnet Composition and Substrate Selection

The film composition is determined by both the lattice parameter of available substrates and by the desired magnetic properties. The magnetization can be controlled by substitution of Ga or Al for Fe in tetrahedral sites, and 0.7-1.5 Ga atoms per formula unit are necessary to reduce the magnetization to 75-150 Gauss. The lattice parameter and magnetic properties, such as domain wall mobility, coercive force and temperature sensitivity, are controlled both by the Ga or Al substitution for Fe and by substitution of rare earth ions in dodecahedral sites, which increase or decrease the mobility by virtue of their specific damping constants and determine the temperature sensitivity of the magnetic properties by their relative contribution to the Néel and compensation

temperatures. The lattice parameter is constrained to match the lattice parameter of the substrate within ±0.015 Å, since increased mismatch causes cracking or faceting of the epitaxial film[12].

Most of the garnet compositions to date have been grown on $Gd_3Ga_5O_{12}$ substrates for two reasons: (1) it has a lattice parameter in the middle of the range of the Ga substituted rare earth iron garnets, which makes it relatively easy to match its lattice parameter; and (2) a great deal of research and development has led to a high degree of perfection of the Czochralski growth process for this garnet so that substrates up to 1.5 inch in diameter are becoming readily available in production quantities with defect densities less than $5/cm^2$. The only disadvantage of this composition is the high cost of gallium oxide, which makes it an expensive material. It would be much cheaper to grow on a non-gallium containing substrate, such as $Y_3Al_5O_{12}$ (YAG), and comparable development in this system would probably result in the same high quality as in the $Gd_3Ga_5O_{12}$ system. Unfortunately, the lattice parameter of YAG is only 12.302 Å, much too small for expitaxial growth of any of the possible bubble garnets, no matter what combination of cations is employed. Another alternative is the development of mixed cation substrates, $(Y,Sm,Gd)_3(Al,Ga)_5O_{12}$, for example, to replace some of the expensive Ga without excessively lowering the lattice parameter. Mixed garnets have been grown, but to date their quality has been inferior to $Gd_3Ga_5O_{12}$, probably because of segregation effects during crystal growth[19].

The HPL materials effort has focused on the use of $Gd_3Ga_5O_{12}$ substrates, which have been purchased from outside vendors. The film

composition has evolved from $(Eu,Er)_3(Ga,Fe)_5O_{12}$ which suffers from low mobility and relatively high coercivity (~80 cm/sec-Oe and 0.5 Oe, respectively) to the $(Gd,Y,Yb)_3(Ga,Fe)_5O_{12}$ compositions which exhibit mobilities higher than 2000 cm/sec-Oe, but are very temperature sensitive, to the $(Sm,Y)_3(Fe,Ga)_5O_{12}$ compositions which have only modest domain wall mobilities of 180-350 cm/sec-Oe, but have excellent temperature stability and satisfy all the requirements for bubble devices. In the last six month period, the materials effort has focused on the $(Sm,Y)_3(Fe,Ga)_5O_{12}$ compositions, and nearly all the results in the following sections of the report will pertain to this material, which appears to be a reasonable compromise between temperature stability and high data rate for bubble devices.

2.5 Solvent Selection

The two solvents used most extensively for the LPE growth of the bubble garnets have been $PbO-B_2O_3$ and $BaO-B_2O_3-BaF_2$. The relative merits and characteristics of each are shown in Table II in relation to the requirements for a good crystal growth solvent listed below.

1. Low vapor or dissociation pressure and low reactivity with the crucible at crystal growth temperatures is desirable, in order to avoid changes in liquid level and composition.
2. The solvent should have a high solubility for the crystal growth constituents, and the metastable supercooled solution should be stable at large supercooling in order to inhibit initial substrate dissolution before heteroepitaxial growth begins.

TABLE II

Properties of PbO-Based and BaO-Based Solvents

	$BaO-B_2O_3-BaF_2$	$PbO-B_2O_3$
Melting Point	750-915°C	< 700°C
Volatility	Negligible at 1250°C	Considerable at 900°C
Viscosity	Relatively high at temperatures less than 1050°C, increases with time at temperatures less than 850°C, > 100 cp	Low down to 800°C, 10-100 cp
Chemical Reactivity with Platinum	Negligible	Reacts readily if free lead is present
Density	Less than magnetic bubble materials ($\sim$ 4.7 gm/cm^3)	Greater than magnetic bubble materials ($\sim$ 6 gm/cm^3)
Solubility of Magnetic Garnets at Growth Temperature	$\sim$ 19 mole % at 1030°C	$\sim$ 10.7 mole % at 940°C
Solvent Incorporation (decreases with increasing temperature)	< 0.1 wt% Ba at 1000°C growth temperature	> 0.6 wt% Pb at 900°C growth temperature
Gallium Distribution Coefficient	$\alpha_{Ga} \approx 0.8-0.9$	$\alpha_{Ga} = 1.6-2.5$
Toxicity	Slight unless ingested	Fumes of PbO are very toxic

3. The liquidus curve (temperature versus composition) should be steep to permit precise control of supersaturation by controlling the solution temperature.
4. The distribution coefficients of the crystal constituents should not vary with temperature to prevent spurious composition fluctuations due to temperature excursions and uneven temperature distribution in the solution during growth.
5. The distribution coefficients as well as the solubility of the solvent ions in the crystal must be very low at the growth temperature to prevent solvent incorporation during growth. This effect can lead to significant changes in composition and lattice parameter in the epitaxial layer.
6. It is desirable for the compound to be congruently saturating to maximize the solute solubility and enhance stoichiometric growth.
7. The solvent should have both a low melting point and a low viscosity to permit growth at as low a temperature as possible.
8. The solvent must wet the substrate and growing crystal, but should also be readily removable from the epitaxial layer after growth.
9. The solution should be readily soluble in common solvents that do not attack the crystal or the growth crucible to facilitate cleaning operations.
10. The solvent should be inexpensive and readily obtainable in high purity form.

The commonly used $PbO-B_2O_3$ solvents fail in Requirements 1, 4, 5 and 6. The BaO-based solvent, on the other hand, has been found to fulfill all the listed requirements except 4 and 6, although it comes closer than the PbO-based solvent, as will be discussed in subsequent sections. The PbO-based solvent appears to have a minor advantage in Requirements 7 and 8.

2.6 Experimental Procedures

2.6.1 Solvent Characterization

2.6.1.1 BaO-Based Solvent

Many of the properties of this solvent have been discussed previously[4,7,20-22], and the discussion here will only summarize the central results. A few liquidus points determined experimentally for the $BaO-B_2O_3-BaF_2$ solvent are shown in Fig. 1. The solvent compositions used most widely during this contract varied from 41% BaO, 41% B_2O_3, 18% BaF_2* to 43% BaO, 41% B_2O_3, 16% BaF_2. No significant variation in film growth or properties was observed for this range of compositions. The solvent was prepared by decomposing $BaCO_3$ in situ with B_2O_3 at 1100-1200°C, and then adding BaF_2 and melting at 1200°C. The total weight loss during the melting and decomposition operations was 0.3-0.4 wt% and was probably due to residual gas and moisture in the B_2O_3 as well as the formation and volatilization of small amounts of BF_3.

The solubility curve for the garnets in this range of solvent compositions is shown in Fig. 2. The relatively high viscosity of the

* All compositions are in mole percent or mole fraction unless otherwise stated.

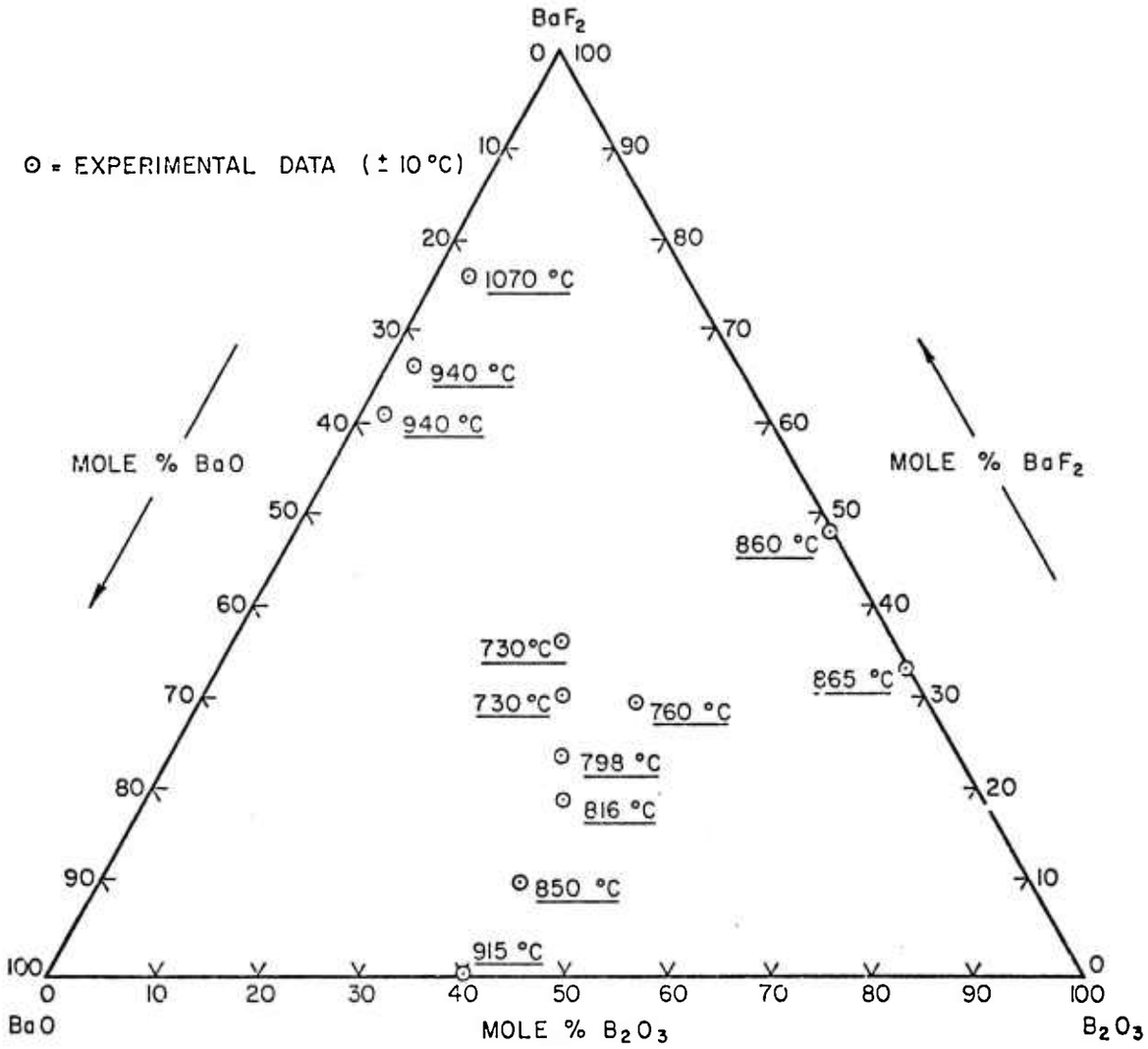

Figure 1. Approximate Liquidus Points for the BaO-B_2O_3-BaF_2 System (the points represent approximate temperatures at which a large qualitative increase in viscosity was noted).

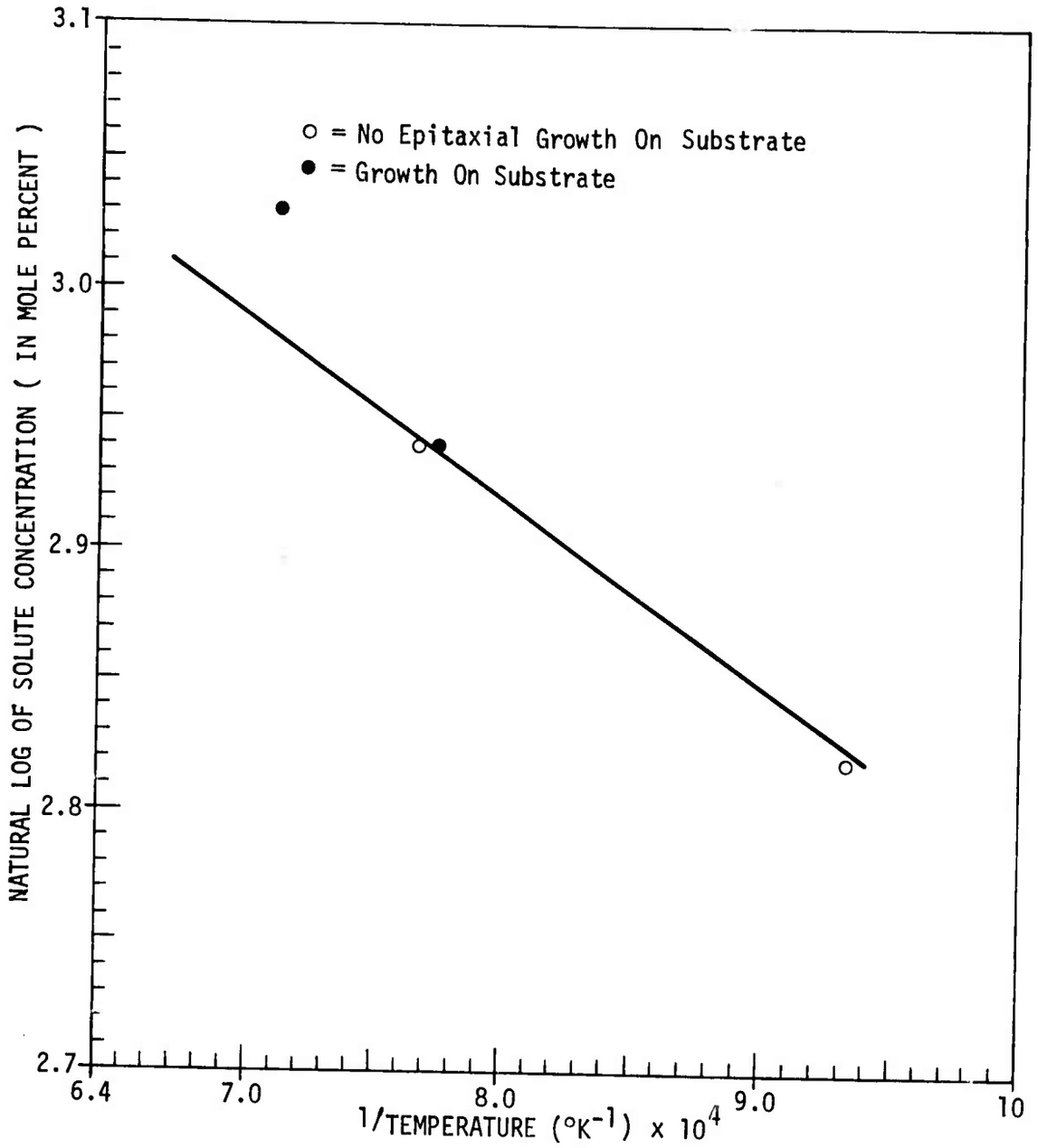

Figure 2. Solubility of $(Sm,Y)_3(Ga,Fe)_5O_{12}$ in $BaO-B_2O_3-BaF_2$ Solvent As Determined by Substrate Dipping Experiments.

solvent coupled with its tendency to wet the garnet surface always left a thin film of solution (a fraction of a micron) on the surface after the substrate was pulled from the solution, usually resulting in a very small amount of garnet growth after removal from the solution. This made it difficult to determine the saturation temperature with precision, and for this reason, the data shown in Fig. 2 are only approximate. The extra growth is negligible compared to the normal film thickness of 3-5 μm and does not have a significant effect on the film properties.

The volatility of the growth solution was measured by placing an uncovered 100 cc crucible containing 250 gm of solution in a muffle furnace at 1250°C for a total of 279 hours. The crucible was taken out of the furnace at intervals and weighed, with the following results.

Time in Furnace (hours)	Time Interval Since Last Weighing (hours)	Weight Loss Since Last Weighing (grams)
15	15	0.2995
30	15	0.0985
45	15	0.1092
60	15	0.0888
171	111	0.3278
186	15	0.0512
279	93	0.4086
Total: 279		1.3836

The average weight loss was 0.005 gm/hr at 1250°C or 0.002 wt% of the solution per hour, which is not enough to significantly affect the saturation temperature. At the conclusion of the experiment, a small sample of the

solution was analyzed by emission spectrographic analysis for Pt, but less than 10 ppm Pt was found, indicating little reaction of Pt with this solvent.

The stability range of the garnet phase is an important parameter for crystal growth. It is desirable to grow the garnet films close to the stoichiometric composition to maximize the usable amount of solute in the solution. Possible foreign phases which could form are the magnetoplumbite phase at high iron concentration, orthoferrite phase at high rare earth concentration and a borate phase (either an iron borate or rare earth borate) due to the relatively large concentration of B_2O_3 in the solution. The results of varying the ratio $R_1 = Fe_2O_3/(Sm_2O_3 + Y_2O_3)$* during the growth of $Sm_{.38}Y_{2.62}Ga_{1.2}Fe_{3.8}O_{12}$ at 1000°C are shown in Table III. The Fe_2O_3/Ga_2O_3 (R_2) and Sm_2O_3/Y_2O_3 ratios were maintained constant at 2.57 and 0.145 during these experiments. At all values of $R_1 > 1.20$, the magnetoplumbite phase formed as red hexagonal platelets lying on top of the epitaxial layer. These platelets appeared in greatest number at the periphery of the film and could be easily removed by scrubbing in alcohol. They probably formed during cooling from the residual solution left on the film after removal from the growth solution. Triangular pits, both flat-bottomed and pyramidal, were also seen in the film. Dark field transmission microscopy at 500X revealed tiny (≤ 0.1 μm) particles embedded in the film beneath many of these pits. For $R_1 \leq 1.08$, no evidence of magnetoplumbite was seen, and the pit density decreased to < 5 pits/cm^2 for $R_1 = 0.80$, increasing again for $R_1 = 0.72$. The particles associated with the pits were too small to quantitatively identify, but may have been a borate phase. Some evidence of an orthoferrite

---

* The nomenclature is that of Blank and Nielsen for PbO-based solutions[23].

TABLE III

Effect of Solute Concentration and Composition Upon
Epitaxial Layer Composition and Second Phase Precipitation for
$Sm_{.38}Y_{2.62}Ga_{1.2}Fe_{3.8}O_{12}$ Grown in 43 (mole)% BaO, 41% B_2O_3, 16% BaF_2

$\frac{\Sigma\ Ln_2O_3\ X100}{\Sigma\ Ln_2O_3 + Fe_2O_3 + Ga_2O_3}$ (mole%)	$R_1 = \frac{Fe_2O_3}{\Sigma Ln_2O_3}$ (mole ratio)	R_4 = Solute Concentration (mole fraction)	Results
30.00	1.68	0.2050	Specular garnet layer, a few red hexagonal platelets, pit density < 100/cm^2
37.50	1.20	0.1900	Specular garnet layer, no red hexagonal platelets, pit density < 20/cm^2
40.00	1.08	0.1900	Specular garnet layer, no red hexagonal platelets, pit density < 20/cm^2.
42.00	0.99	0.1900	Specular garnet layer, no red hexagonal platelets, pit density < 20/cm^2
42.60	0.97	0.1936	Specular garnet layer, no red hexagonal platelets, pit density < 20/cm^2
45.00	0.88	0.1900	Specular garnet layer, no red hexagonal platelets, pit density < 20/cm^2
47.50	0.80	0.1900	Specular garnet layer, pit density 0-5/cm^2
50.00	0.72	0.1900	Specular garnet layer, pit density < 20/cm^2, a few orthorhombic surface features

phase could be seen for R_1 = 0.72 in the form of orthorhombic surface features.

The solubility of the garnet phase increased as the value of R_1 increased, contrary to the behavior reported for the $PbO-B_2O_3$ system[23]. At R_1 = 1.68, for example, no film growth was observed for a solute concentration = 19.5%, although at $R_1 \leq 1.20$ films readily grew at a solute concentration = 19.0%.

The practical range of crystal growth temperatures depended strongly upon the solute concentration, as evidenced by the fact that at an R_1 = 1.1 with 19.0% solute (the conditions under which nearly all the films have been grown), the growth temperature range was 1020-970°C. Below 950°C, large quantities of a borate phase precipitated out, and the solution became mushy. At 16% solute, on the other hand, no garnet growth or second phase precipitation was observed at temperatures as low as 800°C.

2.6.1.2 Comparison with the $PbO-B_2O_3$ Solvent

The PbO-based solvent is much simpler to prepare, since there are no decomposition reactions and it contains only 6 mole% B_2O_3. However, PbO is quite volatile, and the weight loss from 250 gm of solution contained in a loosely covered 100 cc crucible at 1200°C has been measured to be ~0.1 wt%/hr. The weight loss is similar for an open crucible at a normal crystal growth temperature of 900°C and is two orders of magnitude greater than the $BaO-B_2O_3-BaF_2$ solvent. This system is, therefore, difficult to quantitatively characterize, since both the PbO/B_2O_3 ratio and the solute concentration are continuously varying at a fairly rapid rate, leading to complex changes in the saturation temperature[23]. In fact, it is impractical

to use this solvent for LPE growth at 1000°C, just as it is difficult to use the BaO-based solvent at 900°C. The advantage of a higher growth temperature is the decreased amount of solvent incorporation in the garnet due to a decreasing impurity solubility with increasing temperature.

The stability range for garnets in the $PbO-B_2O_3$ solvent has been found to lie somewhere between an R_1 ratio of 14 to 35[23], which is quite iron rich and on the other side of the stoichiometric garnet composition than in the BaO-based solvent. The orthoferrite phase readily forms for $R_1 < 14$, and borates have never been observed in the PbO-based solvent.

The garnet solubility is slightly less at high temperatures for the BaO-based solvent as evidenced by the growth of $(Sm,Y)_3(Fe,Ga)_5O_{12}$ at 1000°C in both solvents. The saturation temperatures were not measured in these experiments, but comparable growth rates ($\sim$0.8 μm/min) were produced for a 16% solute concentration in the PbO-based solution compared to a 19% solute concentration in the BaO-based solution. However, the solubility curve is much steeper in the BaO-based solution as evidenced by the fact that the saturation temperature for a 10.7% solution drops to only 938°C in the PbO-based solution, while the saturation temperature for a 16% solute concentration in the BaO-based solution is less than 800°C.

2.6.2 Substrate Preparation

2.6.2.1 Substrate Processing

$Gd_3Ga_5O_{12}$ substrate blanks were purchased from outside vendors and polished in-house. A preliminary lapping operation was performed with alumina to remove saw damage and flatten the substrates, followed by a

prepolish with 0.3μm alumina and a standard Syton* polish[22], which removed 0.3 mil and left little or no damage to the surface. The polished substrates were ultrasonically cleaned with a detergent solution followed by a final rinse in organic solvents.

2.6.2.2 Substrate Characterization and Evaluation

Substrate lattice parameters were measured by the Debye-Scherrer and single crystal X-ray diffractometry techniques described in Ref. (22), and were found to be in the range of 12.379-12.384 Å. The substrate orientation was determined by Laue X-ray diffraction analysis to be {111} ±1°.

Defects in the substrates, such as dislocations, growth striations, inclusions and the core defect (caused by the formation of {211} and {110} facets on the growth interface) were studied by a variety of techniques, including optical observation of the birefringence associated with such defects, etch pitting, and Lang and Berg-Barrett X-ray topographic techniques.

The techniques and observations have been extensively described in earlier reports[22]. During the last contract period, the substrate quality improved to the point where the substrate characterization was needed only periodically as a routine quality check, and substrates containing > 10 defects per cm^2 were rejected for LPE growth.

---

* A product of Monsanto Company.

2.6.3 Crystal Growth

2.6.3.1 LPE Growth in $BaO-B_2O_3-BaF_2$ and $PbO-B_2O_3$ Solvents

During this contract period, all LPE growth was performed by the horizontal dipping technique with a rotating substrate as shown in Fig. 3. Only one substrate was dipped at a time, and in some cases the substrate was lowered only to the surface of the solution and rotated. This produced a film on only the bottom surface, which was useful both for ease of domain observation and magnetic measurements, as well as conserving solute to extend the useful life of the solution. A platinum furnace with a 4 inch bore was used for the LPE growth, and a 100 cc standard form cp grade platinum crucible was filled with 30 cc of solution. This produced a liquid depth of 2 cm in the crucible, which was placed in a 4-inch isothermal zone (±2°C) in the furnace. Experimental conditions for growth from $PbO-B_2O_3$ solutions were identical except that a Kanthal* wound furnace was used. Solution compositions for the growth of $Sm_{.38}Y_{2.62}Ga_{1.2}Fe_{3.8}O_{12}$ are given in Table IV.

The $Gd_3Ga_5O_{12}$ substrates were mounted in a 3-pronged platinum holder attached to an alumina rod and were placed just above the solution for 10 minutes to adjust to the furnace temperature before insertion into the liquid. The substrates were continuously rotated in the furnace at rates of 10-600 rpm. After growth, the substrates were raised 5 mm above the liquid surface and rotated at 2250 rpm in the BaO-based solvent and 500 rpm in the PbO-based solvent to remove most of the solution. The high speed rotation time in the BaO-based solvent was varied from 15 sec to 6 min, to

---

* A product of the Kanthal Corporation.

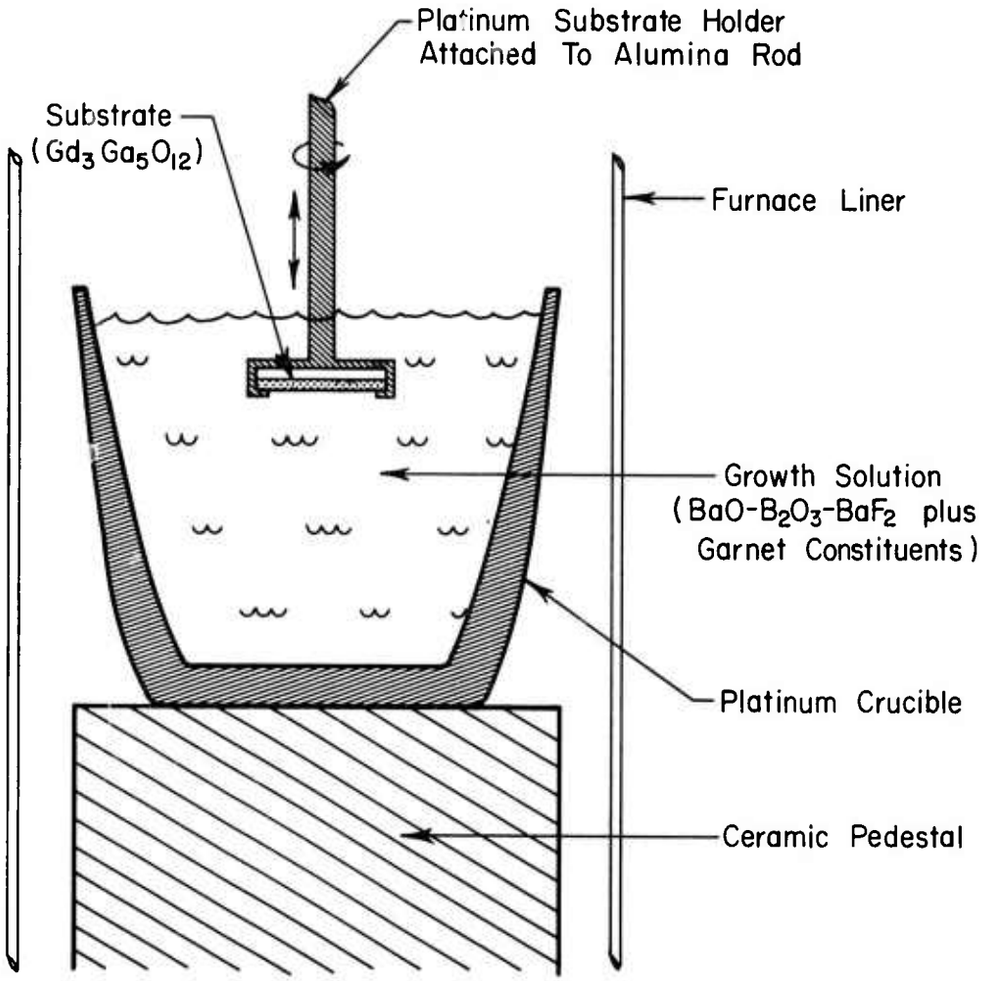

Figure 3. Liquid Phase Epitaxial Growth Apparatus.

TABLE IV

Solution Composition for the Growth of $Sm_{.38}Y_{2.62}Ga_{1.2}Fe_{3.8}O_{12}$ in BaO-Based and PbO-Based Solvents

	Growth Temp. = 1000°C	Growth Temp. = 900°C
BaO	47.6548 gm	-
B_2O_3	20.4457	4.6116
BaF_2	20.6971	-
PbO	-	230.7500
Sm_2O_3	3.3514	0.1994
Y_2O_3	14.9658	0.8906
Fe_2O_3	10.6636	17.4670
Ga_2O_3	4.8673	3.2270
R_1	0.88	24.22
R_2	2.57	6.35
R_3	-	15.61
R_4	0.1900	0.1065

$$R_1 = \frac{Fe_2O_3}{\Sigma Ln_2O_3} \qquad R_3 = \frac{PbO}{B_2O_3}$$

$$R_2 = \frac{Fe_2O_3}{Ga_2O_3} \qquad R_4 = \frac{\text{Solute}}{\text{Solute + Solvent}}$$

determine the minimum time required to get enough solution off to avoid cracking or spalling the epitaxial layer. The optimum time seemed to be 1-2 minutes, after which there remained a very thin film of solution over the whole epitaxial layer with slight buildup at the substrate holder. At longer times, the surface of the epitaxial layer began to roughen, presumably due to rapid growth of the small amount of solution remaining on the surface, and for shorter times, there was a high probability of substrate cracking, caused by a film of solution on the top and bottom sides of the substrate at its periphery. Since the thermal expansion coefficient of the solvent is only one-third that of the garnet[24], the stresses induced during cooling invariably cracked the substrate when there was an excess of solution remaining on the layer. The crack always started at the drop of solution remaining at the periphery and often only propagated partially across the wafer. However, substrate cracking and spalling was completely eliminated by proper post-growth, high-speed spinning.

2.6.3.2 Control and Reproducibility in the BaO-Based Solvent

A series of growth runs were performed with growth time, rotation rate and growth temperature as parameters, to determine their effect upon growth rate and properties of the films. A straightforward analysis based upon diffusion of solute through a uniform boundary layer adjacent to a rotating disk predicts a steady-state flux of nutrients through the boundary layer following an initial transient[15]. The experimental film thickness as a function of growth time for $(Sm,Y)_3(Fe,Ga)_5O_{12}$ grown at 1000°C with a rotation rate of 120 rpm is shown in Fig. 4. The supercooling was 30°C for

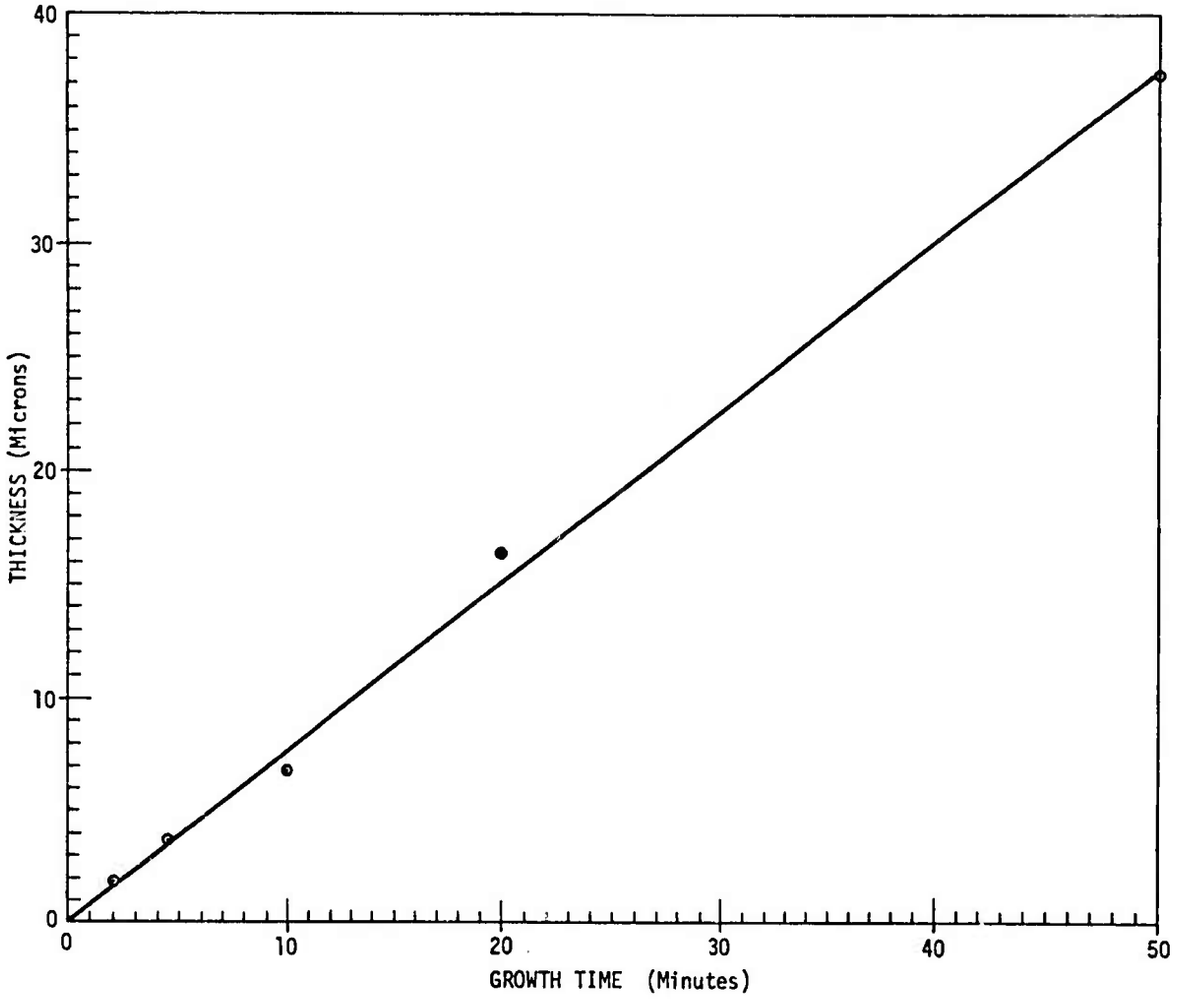

Figure 4. Growth Rate for $(Sm,Y)_3(Ga,Fe)_5O_{12}$ Grown in $BaO-B_2O_3-BaF_2$ Solvent at 1000°C, 120 rpm. Solute Concentration = 19.00 mole%, $T_{sat} \sim 1030°C$.

this series of runs and it can be seen that the straight line relationship extrapolates back to the origin, indicating that the initial transient is too short to be seen on this time scale. Calculations by Ghez and Giess[25] indicate that the initial transient for the $PbO-B_2O_3$ solvent is also very short, of the order of 1 second. The solution stability is shown by the fact that the datum for a growth time of 50 minutes also lies on the straight line, indicating no spontaneous nucleation occurring elsewhere in the solution during this time.

The theory also predicts a linear variation of growth rate with the square root of rotation rate, and this relationship is demonstrated experimentally in Fig. 5. The linear variation holds from 0-600 rpm for the BaO-based solvent.

The growth rate variation with supercooling is shown in Fig. 6, where the growth temperature was varied from the saturation temperature of $\sim$ 1030°C to 960°C (a maximum supercooling of 70°C). The variation is linear up to 50°C supercooling, beyond which spontaneous nucleation of garnet crystals occurs in the solution as evidenced both by the drastic reduction in growth rate as well as optical observation of many small garnet crystals growing on the surface of the epitaxial film.

Reproducibility of film properties has been demonstrated in a previous report[14] and is shown for the $(Sm,Y)_3(Fe,Ga)_5O_{12}$ composition in Table V. Here all growth parameters have been kept constant for a series of growth runs after one initial run to determine the parameters to generate the required film properties. The growth temperature was 1000°C ±1°C, growth time 11 minutes ±10 seconds and rotation rate 120 rpm ±2 rpm. The solution

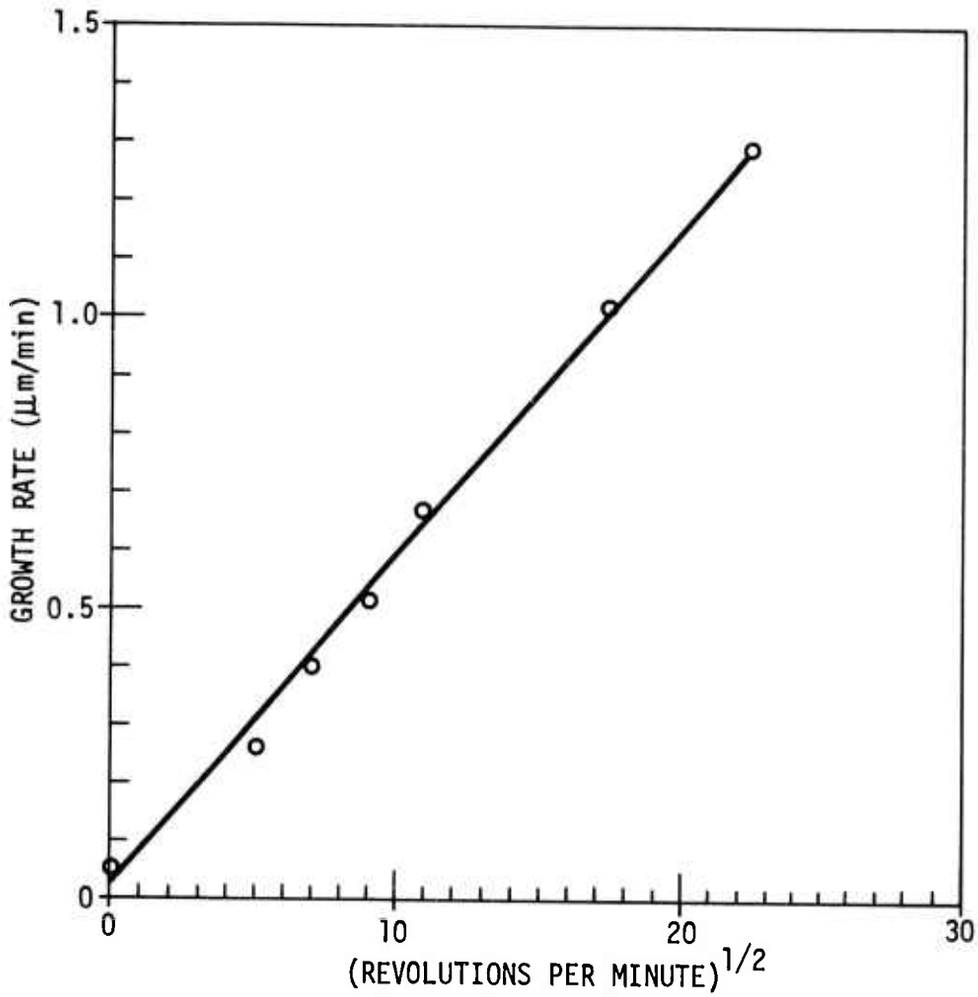

Figure 5. Growth Rate Dependence on Rotation Rate for $(Sm,Y)_3(Ga,Fe)_5O_{12}$ Grown in $BaO-B_2O_3-BaF_2$ Solvent at 1000°C. Solute Concentration 19.00 mole%, $T_{sat} \sim 1030$°C.

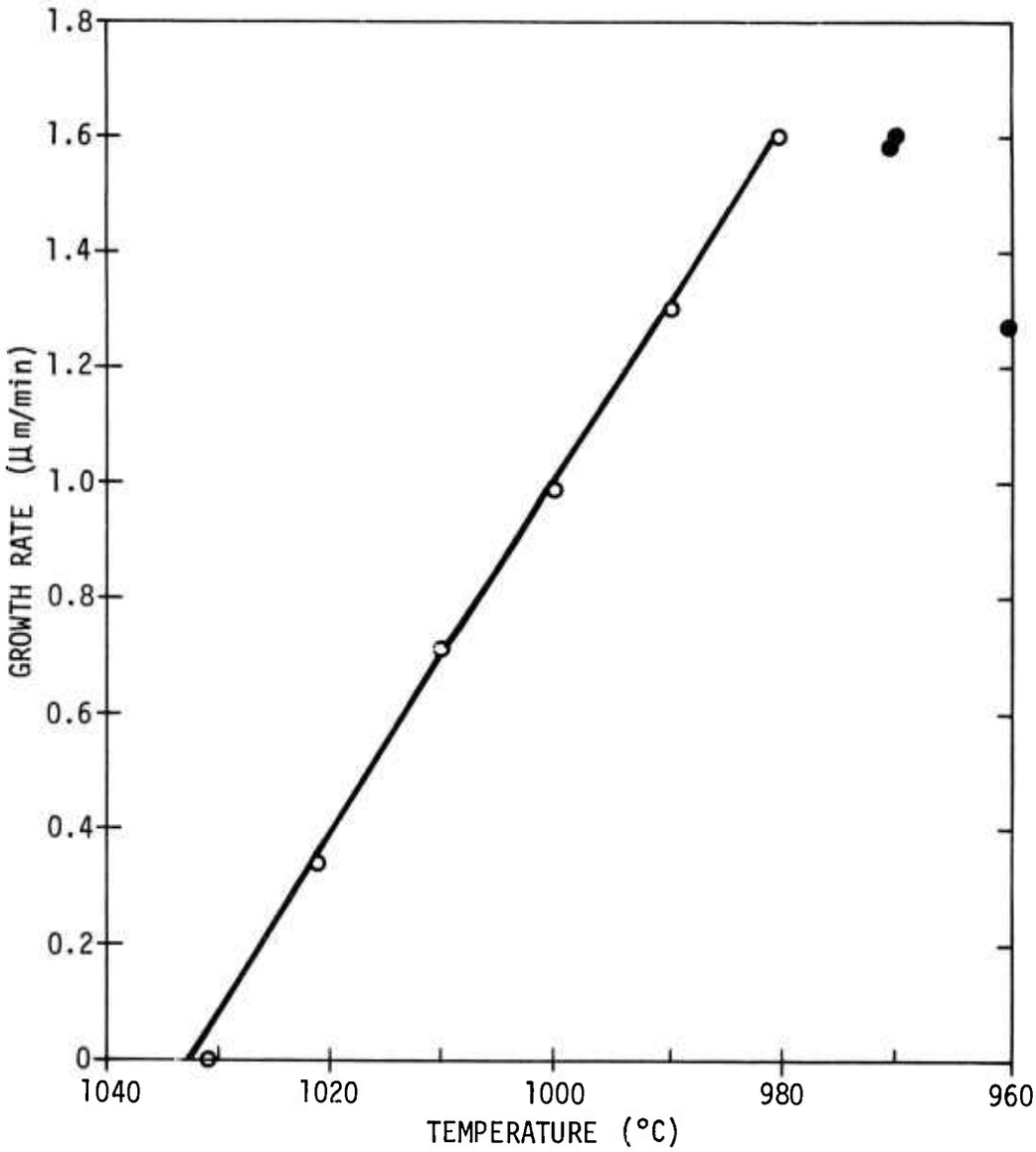

Figure 6. Growth Rate Dependence on Supercooling for $(Sm,Y)_3(Ga,Fe)_5O_{12}$ Grown in $BaO-B_2O_3-BaF_2$ Solvent at 300 rpm Rotation Rate. Solute Concentration = 19.00 mole%, $T_{sat} \sim 1030°C$. (Blackened circles indicate spontaneous nucleation.)

TABLE V

Reproducibility Data for $Sm_{.38}Y_{2.62}Ga_{1.2}Fe_{3.8}O_{12}$ Grown in $BaO-B_2O_3-BaF_2$ Solvent

Run No.	Thickness (μm)	Characteristic Length (μm)	Magnetization (Gauss)	Collapse Field (Oe)	Wall Energy (ergs/cm^2)
1	1.6	-	-	-	-
2	5.1	0.89	139	58.3	0.14
3	4.4	0.84	133	52.4	0.12
4	5.4	0.73	120	57.2	0.08
5	5.0	0.82	125	53.7	0.10
6	5.3	0.86	130	57.0	0.12
7	5.3	0.86	130	57.0	0.12
8	5.4	0.85	130	58.3	0.12
9	5.7	0.88	129	57.5	0.12
10	5.7	0.90	135	59.3	0.13
11	5.4	0.91	124	53.3	0.11
12*	5.3	0.88	142	59.7	0.14
13	5.1	0.90	128	53.4	0.12
14*	5.2	0.84	125	54.5	0.10
15	5.1	0.89	130	54.8	0.12
16*	4.6	0.87	131	51.6	0.12
17	5.4	0.89	128	55.7	0.12
18*	4.4	0.88	128	49.4	0.12
19	5.2	0.90	124	52.4	0.11
20*	5.0	0.90	129	54.0	0.12
21	5.0	0.93	121	49.0	0.11
22*	4.7	0.88	127	50.8	0.11
23	4.6	0.97	121	55.4	0.11
24*	4.4	0.92	126	47.2	0.12
25	5.0	0.91	121	49.4	0.11
26*	4.4	0.91	127	47.4	0.12
27	4.9	0.96	121	45.9	0.11
28*	4.1	0.92	136	45.7	0.14
Average Values for 20 runs (Runs 2-21)	5.2	0.87	129	54.8	0.115
Percentage Yield for ±5% Variation from Average	75%	95%	85%	70%	70%

* Growth runs performed immediately after preceding run without a 1200°C equilibration.

was stirred continuously at 1200°C overnight and on weekends, and then brought down to the growth temperature of 1000°C by automatic set point control over a 90-minute period. Growth was initiated when the measuring thermocouple adjacent to the crucible reached a certain value, and the cool down time required to reach this value was constant ±6 minutes. For most of the runs, the temperature was brought up to 1200°C between the runs except for those marked with an asterisk, which took place immediately after the preceding run without any equilibration at 1200°C.

Film thicknesses were determined by fringe counting techniques as well as metallographic examination, and the estimated accuracy was ±5%. The characteristic length was determined by measuring the equilibrium stripe width together with film thickness, and the accuracy was again ±5%. The uncertainty in the collapse field and magnetization was ±0.5 Oe and ±10%, respectively. The results indicate that for the first twenty runs, the yield for ±5% variation in properties from run to run was 75% for thickness, 95% for characteristic length, 85% for magnetization and 70% for collapse field. These results were accomplished in only 30 cc of solution, and the reproducibility may be expected to improve with larger solution volume.

2.6.3.3 Control and Reproducibility in PbO-Based Solvents

The effect of growth parameters upon growth rate and film properties of $(Sm,Y)_3(Fe,Ga)_5O_{12}$ were studied in the $PbO-B_2O_3$ solvent in the temperature range 930-860°C. The film thickness as a function of time is shown in Fig. 7 for a supercooling of 38°C, and it can be seen that there was no spontaneous nucleation even for growth times of 100 minutes.

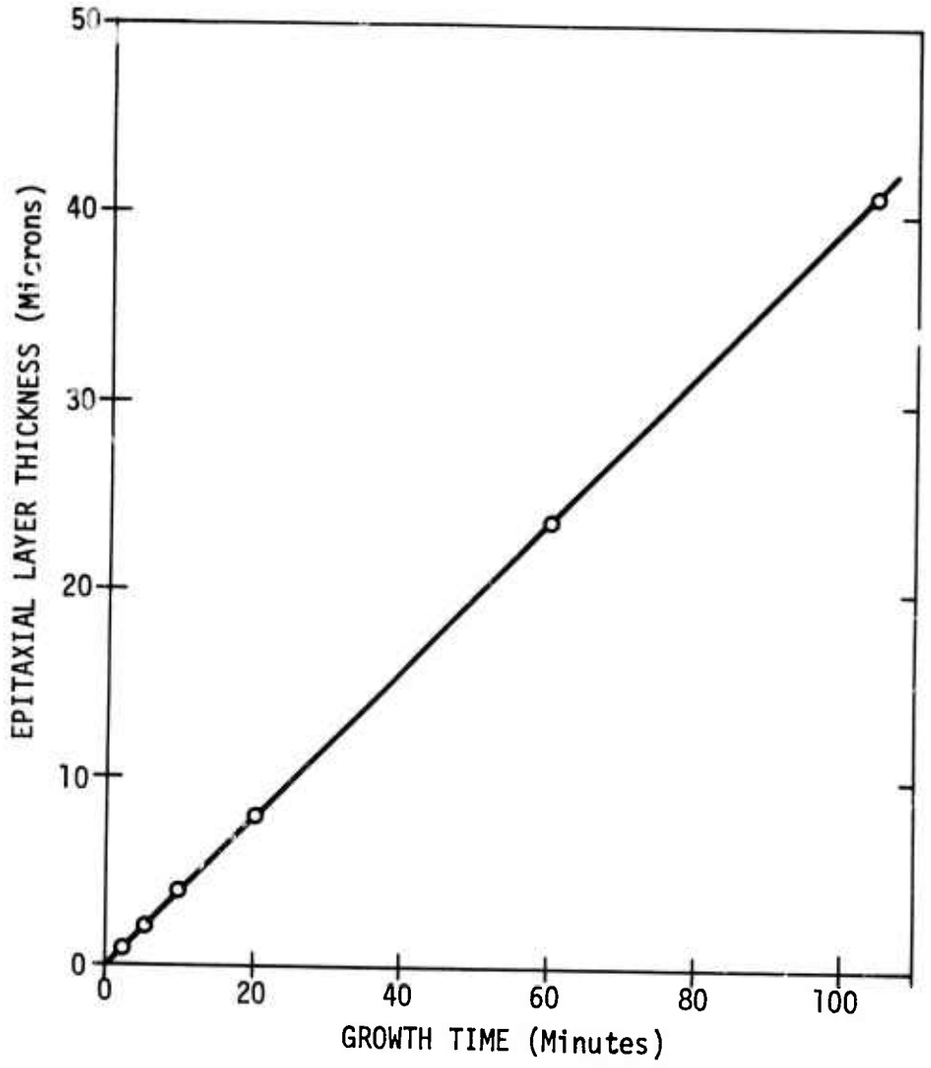

Figure 7. Growth Rate for $(Sm,Y)_3(Ga,Fe)_5O_{12}$ Grown in $PbO-B_2O_3$ Solvent at 900°C, 100 rpm Rotation Rate. Solute Concentration 10.65 mole%, $T_{sat} \sim 938°C$.

The dependence of growth rate upon rotation rate is shown in Fig. 8, which again agrees fairly closely with theoretical expectations[15]. Figure 9 demonstrates the linear variation of growth rate with supercooling up to a supercooling of 38°C, beyond which the growth rate drops off drastically due to spurious nucleation in the solution.

The film property variation for a series of reproducibility experiments is shown in Table VI for a $(Gd,Y,Yb)_3(Fe,Ga)_5O_{12}$ garnet. During this series of experiments, the growth parameters were not held constant, but rather a very close feedback was established so that the magnetic properties and thickness of the film were usually (but not always) measured before each successive growth run, and the growth parameters were then adjusted accordingly.

2.6.3.4 Comparison of the Growth Process in BaO- and PbO-Based Solvents

The data shown in the preceding sections clearly indicate that there is no fundamental difference in crystal growth kinetics between the $BaO-B_2O_3-BaF_2$ and the $PbO-B_2O_3$ solvent systems, and that both obey the growth model most recently formulated by Giess, et al.[15] The major differences lie in some of the more practical aspects of crystal growth.

The useful range of growth temperatures is higher for the BaO-based solution because its viscosity increases rapidly with decreasing temperature, while the volatility and Pt solubility in the PbO-based solution become a problem at higher temperatures. Thus, the $BaO-B_2O_3-BaF_2$ solvent can be used at temperatures above 950°C. This is advantageous from the viewpoint of solvent incorporation in the garnet film, since the solubility

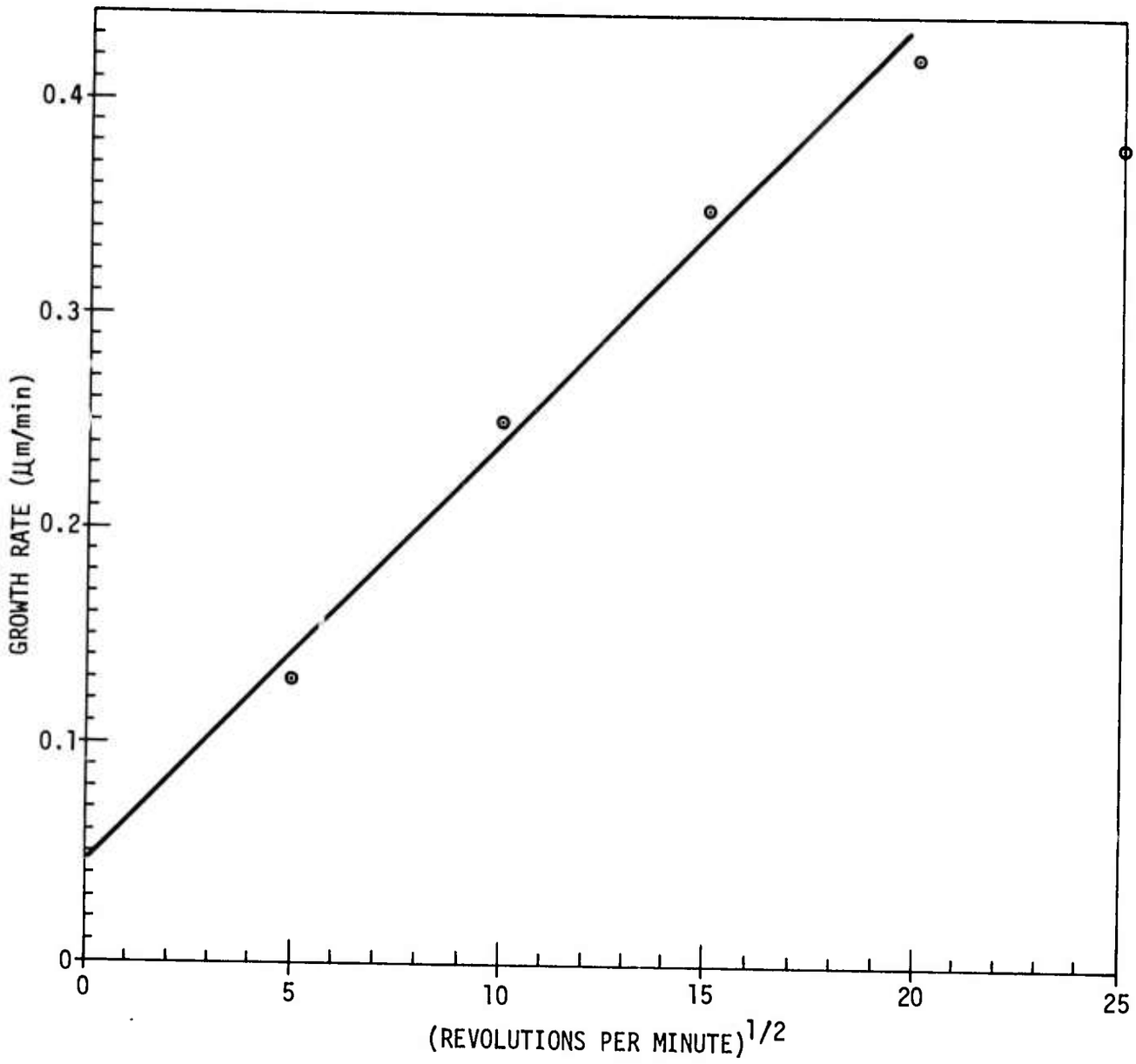

Figure 8. Growth Rate Dependence on Rotation Rate for $(Sm,Y)_3(Ga,Fe)_5O_{12}$ Grown in $PbO-B_2O_3$ Solvent at 900°C. Solute Concentration 10.65 mole%, $T_{sat} \sim 938°C$.

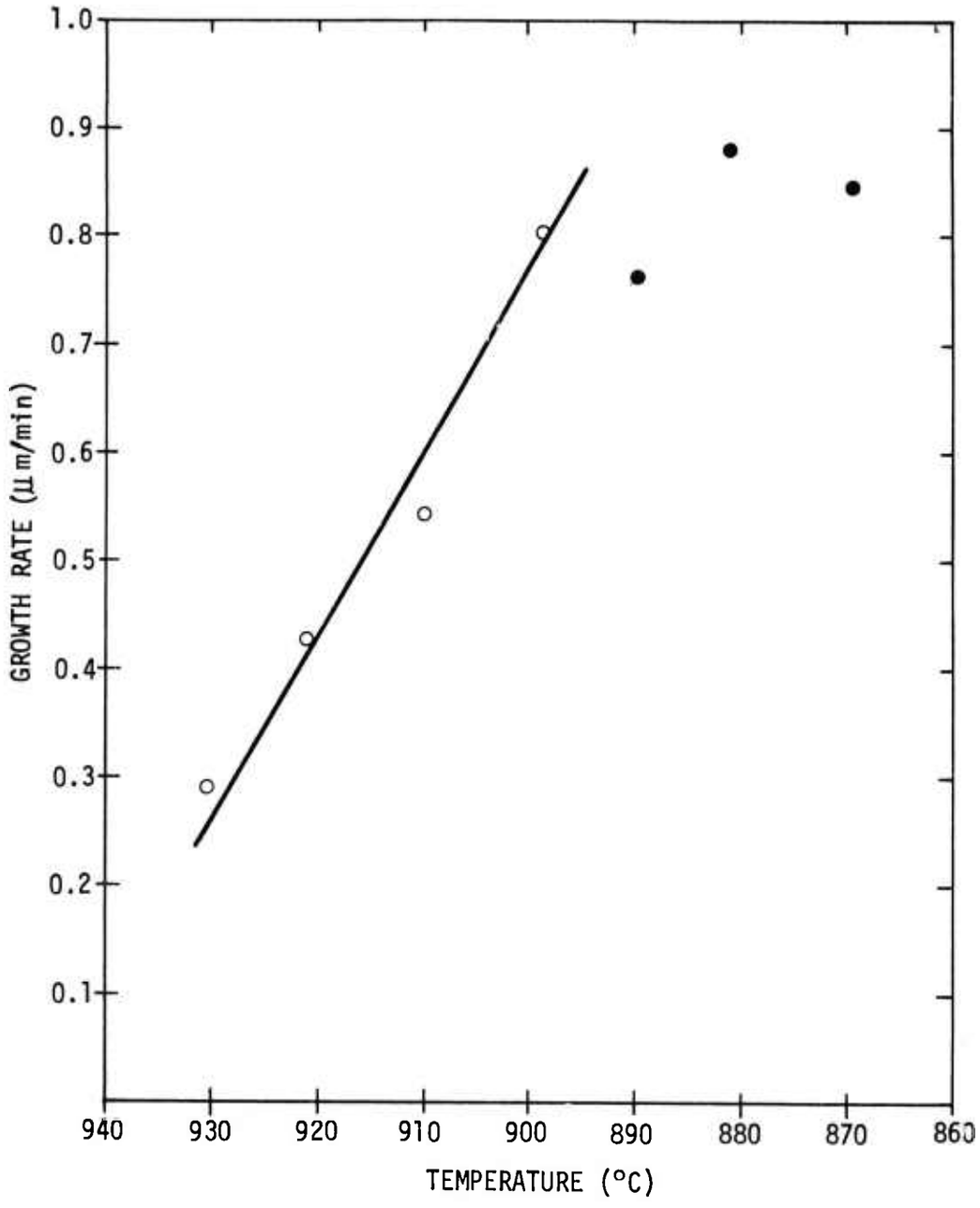

Figure 9. Growth Rate Dependence on Supercooling for $(Sm,Y)_3(Ga,Fe)_5O_{12}$ Grown in $PbO-B_2O_3$ Solvent, 100 rpm Rotation Rate. Solute Concentration = 10.65 mole%, T_{sat} = 938°C. (Blackened circles indicate spurious nucleation in the solution.)

TABLE VI

Reproducibility Data for $Gd_{.8}Y_{1.6}Yb_{.6}Ga_{.9}Fe_{4.1}O_{12}$ Grown in $PbO-B_2O_3$ Solvent

Run No.	Temp. (°C)	Time (min)	Rotation Rate (rpm)	Thickness (μm)	Char. Length (μm)	4πM (Gauss)	Collapse Field (Oe)
1	900	7.0	50	5.7	0.74	115	-
2	900	5.0	50	4.0	0.90	135	48.0
3	900	5.0	50	3.4	0.94	139	42.0
4	900	4.25	100	4.2	0.88	147	55.0
5	900	4.5	100	4.2	0.89	146	55.0
6	895	4.0	100	3.8	0.83	153	54.0
7	895	4.33	100	4.0	0.85	146	54.0
8	895	4.33	100	3.8	0.81	151	56.0
9	895	4.33	100	3.6	0.77	160	59.0
10	895	4.5	100	4.1	0.80	150	57.0
11	895	4.5	100	3.7	0.80	160	58.5
12	895	4.5	100	4.8	0.94	148	58.0
13	895	4.5	100	3.6	0.82	152	54.0
14.	895	4.5	100	4.2	0.86	149	56.0
15	895	4.75	100	3.9	0.82	152	56.4
16	895	4.75	100	3.6	0.80	160	57.0
17	895	4.75	100	3.4	0.81	174	59.0
18	895	4.75	100	3.6	0.82	153	54.0
19	895	5.0	100	3.9	0.84	143	52.5
20	895	5.0	100	3.6	0.78	160	58.5
21	895	5.0	100	3.6	0.81	156	55.5
22	895	5.0	100	4.1	0.84	152	58.0
23	895	5.0	100	3.6	0.85	150	51.0
24	895	5.0	100	4.4	0.80	150	61.0
25	895	5.0	100	3.9	0.87	141	50.5
26	895	5.0	100	3.5	0.96	152	46.5
27	895	5.0	100	fell into solution			
28	895	5.0	100	3.1	0.86	146	43.5
29	890	5.0	100	3.2	0.87	141	43.5
30	885	5.0	100	3.6	0.82	140	49.0
31	885	5.0	100	2.9	0.78	155	48.0
Average for 20 runs (Runs 2-21)				3.8	0.84	152	55.0
Percentage Yield for ±5% Variation from Average				70%	70%	60%	65%

of both Pb and Ba decreases with increasing temperature[22], and in the case of Pb, the amount of incorporation ranges from 1 wt% at 900°C to 0.1 wt% at 1000°C, while the incorporation of Ba has been measured to be < 0.1 wt% at 1000°C.

The viscosity of the BaO-based solvent is higher than that of the PbO-based solvent, and this appears to have an effect on the film flatness (at least for the crucible geometry used in this program). The films grown in the BaO-based solvent are thickest in the central region with concentric interference fringes proceeding to the periphery. The diameter of the first fringe is rotation dependent and varies from 7 mm for 120 rpm to 10-12 mm for 300 rpm rotation rate. This is probably due to edge effects produced by fluid inertia between the film periphery and the crucible wall. The flatness of films grown in the PbO-based solvent, on the other hand, is relatively independent of rotation rate (in the 30-300 rpm range) in the central portion of the film. The thickness uniformity obtained on 1.2 inch diameter substrates in a 100 cc crucible is shown in Figs. 10 and 11. The film thickness uniformity can probably be improved in the BaO-based solvent by using larger diameter crucibles.

Solution removal after crystal growth is accomplished by a high speed rotation just above the surface. The higher viscosity of the BaO-based solvent makes the removal process more difficult, but nearly all the solution can be removed by rotation at 2250 rpm for 1 minute. Solution removal in the PbO-based solution can be effected by rotation at 200-500 rpm but is more sensitive to vibration, since droplets at the periphery were observed to break up and move toward the center of the layer when holder vibration was present.

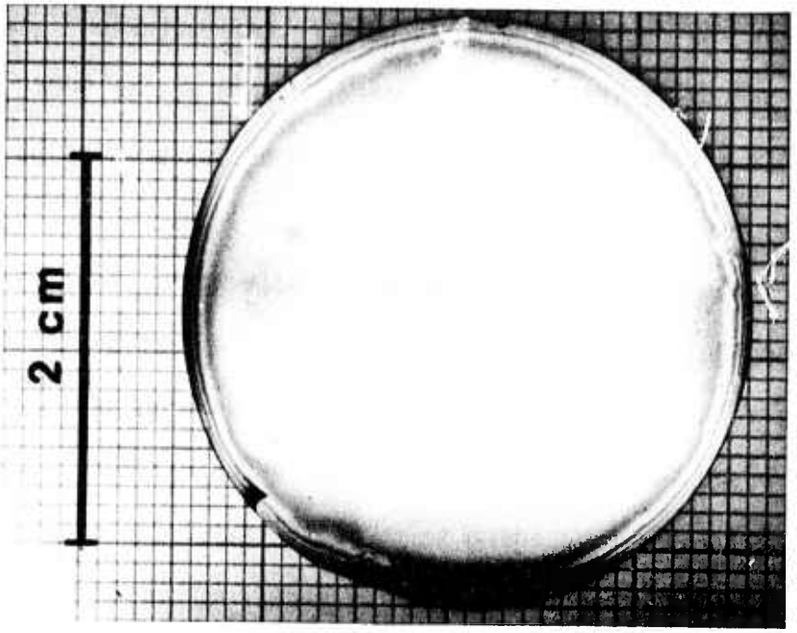

Figure 10. Thickness Uniformity in $(Sm,Y)_3(Ga,Fe)_5O_{12}$ Grown in $PbO-B_2O_3$ Solvent. Sodium Illumination (Each Fringe = 0.13 μm Difference in Thickness). Film Thickness = 4 μm.

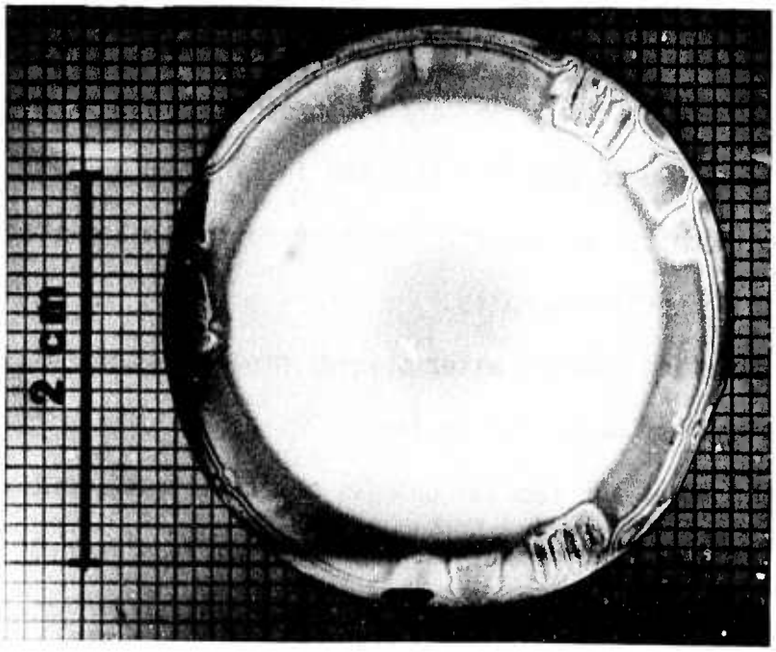

Figure 11. Thickness Uniformity in $(Sm,Y)_3(Ga,Fe)_5O_{12}$ Grown in $BaO-B_2O_3-BaF_2$ Solvent. Sodium Illumination (Each Fringe = 0.13 μm Difference in Thickness). Film Thickness = 3.5 μm.

The stability range for the garnet phase in terms of the rare earth-iron oxide ratio is closer to the stoichiometric composition for the BaO-based solvent than it is for the PbO-based solvent, which, together with the higher growth temperatures, allows a much higher solute concentration in the BaO-based solution (19% for 1000°C growth temperature compared to 12% for a 900°C growth temperature in the PbO-based solution). The higher solute content of the solution and the very low volatility of the BaO-based solvent provide much better run to run reproducibility in this solution than in the PbO-based solution.

SECTION III

3.0 FILM CHARACTERIZATION

Film characterization is essential to an understanding of the growth process as well as an evaluation of the films for use in bubble devices. A list of characterization procedures utilized at HPL is shown in Table VII. Details of the techniques have been described elsewhere[22] and the discussion below is primarily limited to the results of the characterization.

3.1 Defects in the Garnet Films

The epitaxial layers should be defect free to ensure successful device operation, since all common crystallographic defects will markedly increase the local coercive force in the material. Defects arise from three sources: (1) substrate defects such as dislocations or inclusions which are propagated into the epitaxial film during growth, (2) processing defects including substrate scratches and debris left from the cleaning process, and (3) particles or inclusions in the film itself arising from a contaminated solution or spurious nucleation during growth. A detailed discussion of defects and their origin has been recently given by Miller[26]. Substrate defects are becoming uncommon, since $Gd_3Ga_5O_{12}$ can now be routinely grown nearly inclusion and dislocation free with no central core defect. The Syton polishing process has become standardized, and with reasonable care involving clean room procedures, the surfaces can be cleaned to less than five defects per cm^2. Any residual defects are usually dust particles on the surface. The most troublesome defect occurs during crystal growth in

Table VII.

Characterization Techniques for Magnetic Rare Earth Iron Garnets

Parameter	Current HPL Method	Estimated Error in Analysis
1. Substrate and film surface perfection	Etch pit studies, Berg-Barrett and Lang topography, optical microscopic mapping, scanning electron microscopy	-
2. Impurity analysis	Emission spectroscopy, microprobe analysis	±10%
3. Film composition and compositional homogeneity	Microprobe, lattice parameter measurement, calculate from magnetization and Neél temperature	±10%
4. Film-substrate lattice parameter difference and film lattice parameter	X-ray diffractometry	Varies from ± .001Å to ± .005Å depending on mismatch
5. Film thickness and thickness uniformity	Metallographic cross section, interferometry	±10%
6. Magnetization	Static collapse of bubbles, Stripe domain width	±15%
7. Characteristic length	Stripe domain width	±5%
8. Wall energy	Calculate from $\sigma_w = 4\pi M^2 \ell$	±15%
9. Anisotropy constants	Torque magnetometer	±20%
10. Mobility	Bubble translation	±20%
11. Coercive force	AC optical modulation, bubble translation	±15%
12. Neél Temperature	Faraday effect domain observation in hot stage microscope	±1°C
13. Stripe width temperature coefficient	Faraday effect domain observation in hot stage microscope	±10%
14. Index of refraction	Brewster angle	±5%

the form of either second phase precipitates or spontaneously nucleated garnet crystals on the film. In both the BaO-based and the PbO-based solvents, the stablity regime for the garnet phase is limited. If the solution is too rare earth oxide rich, orthoferrite crystals precipitate out, and if it is too iron oxide rich, magnetoplumbite crystals appear. Both these phases are magnetic and interfere with motion of the magnetic domains. In addition, in the BaO-based solvent, some evidence of an additional borate phase has been detected as discussed in Section 2.6.1.1.

Some examples of pits and associated inclusions in a 55 μm thick film of $(Sm,Y)_3(Fe,Ga)_5O_{12}$ grown in $PbO-B_2O_3$ are shown in Figs. 12-16. The surface manifestations are shown in Fig. 12, where they appear as shallow triangular pits in bright field reflected light. Dark field transmitted light reveals faceted reddish precipitates about 30 μm below the surface as shown in Fig. 13. SEM micrographs of a cleaved surface are shown in Figs. 14 and 15. The garnet crystals can be seen in the two holes on the right, while the third has fallen out of the hole on the left. These crystals are about 16 μm in diameter, and appear to have spontaneously nucleated after 10 μm of growth of the epitaxial layer. The surface pits associated with the inclusions can also be seen in Fig. 14. The interaction of these inclusions with the magnetic domain structure is shown in Fig. 16.

Examples of the magnetoplumbite phase and the pit morphologies seen in films grown in the BaO-based solvent are shown in Figs. 17 and 18. These growth defects in both the BaO-based and the PbO-based solvents can be suppressed by careful choice of the iron oxide/rare earth oxide ratio (R_1), by limiting the supercooling to less than 15-20°C and by growing the epitaxial

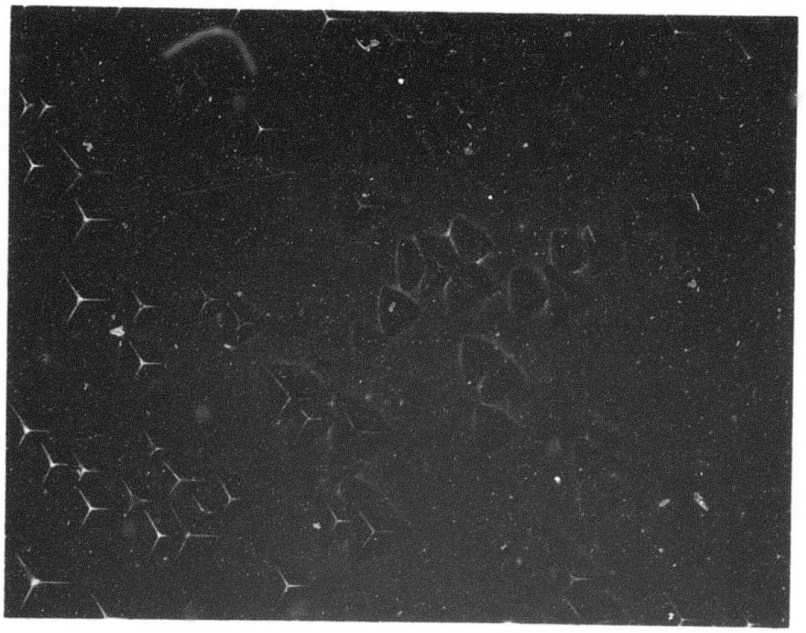

Figure 12. Surface Pits in $(Sm,Y)_3(Ga,Fe)_5O_{12}$ Epitaxial Layer 55 μm Thick, Grown in $PbO-B_2O_3$ Solvent at 900°C. 200X, Bright Field Reflected Light.

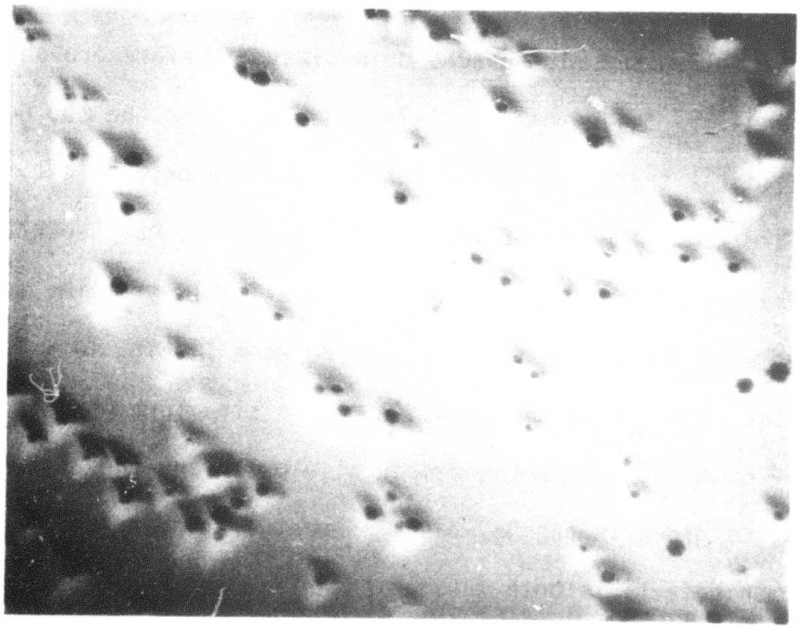

Figure 13. Same Area as Fig. 12, Dark Field Transmitted Illumination, Focused About 30 μm Below Surface of the Epitaxial Layer (200X).

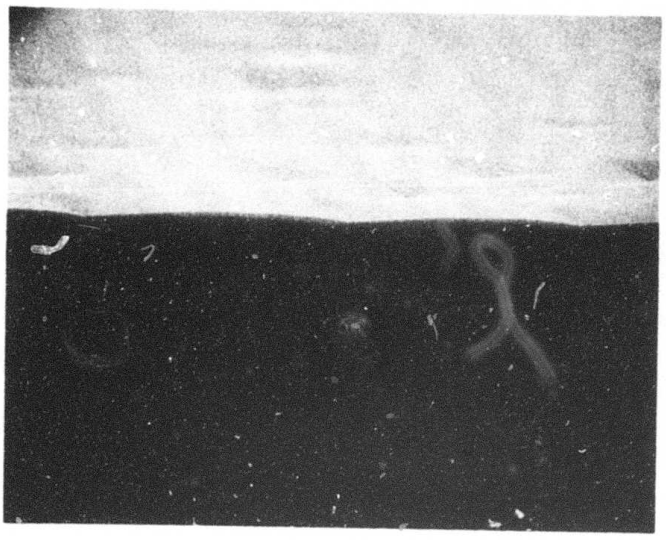

Figure 14. SEM Photograph of Fractured Section of the Epitaxial Layer Shown in Figs. 12 and 13. Substrate is at the Bottom and the Top Surface of the Layer is Visible at the Top. Incident Angle 80°, 500X.

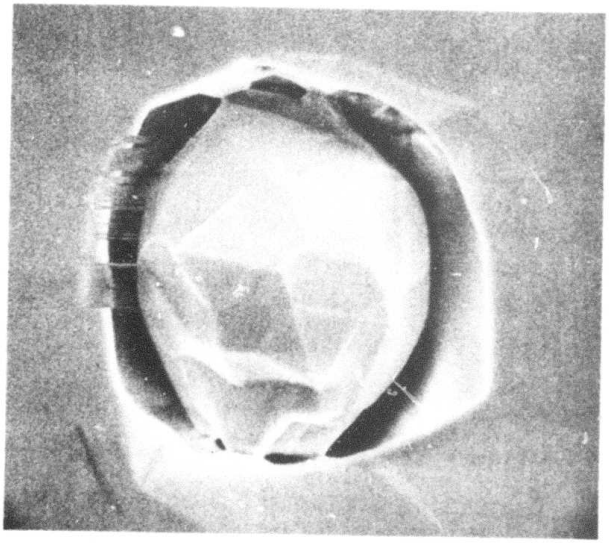

Figure 15. SEM Photograph of the Inclusion at the Right in Fig. 14. 3000X. (There are slight charging effects at the left.)

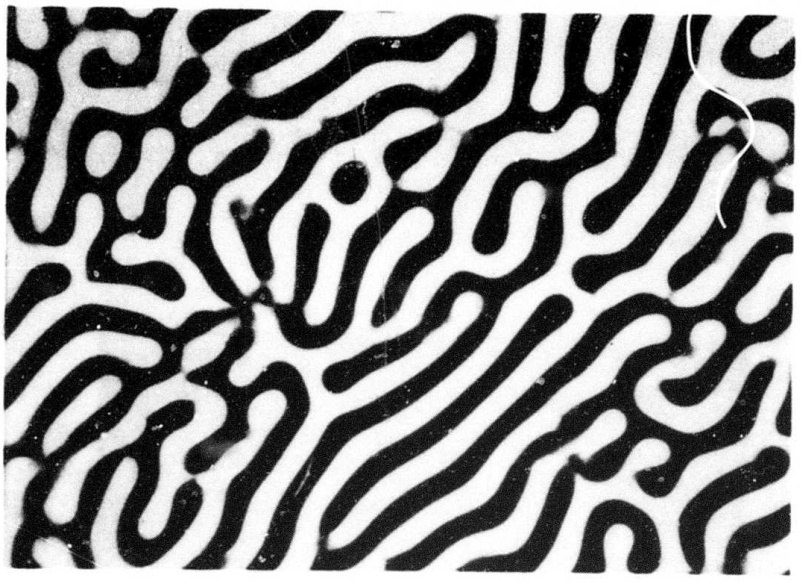

Figure 16. Interaction of Magnetic Domains with Defects in the Epitaxial Layer of $(Sm,Y)_3(Ga,Fe)_5O_{12}$ Shown in Figs. 12-15. Polarized Transmitted Illumination, 200X.

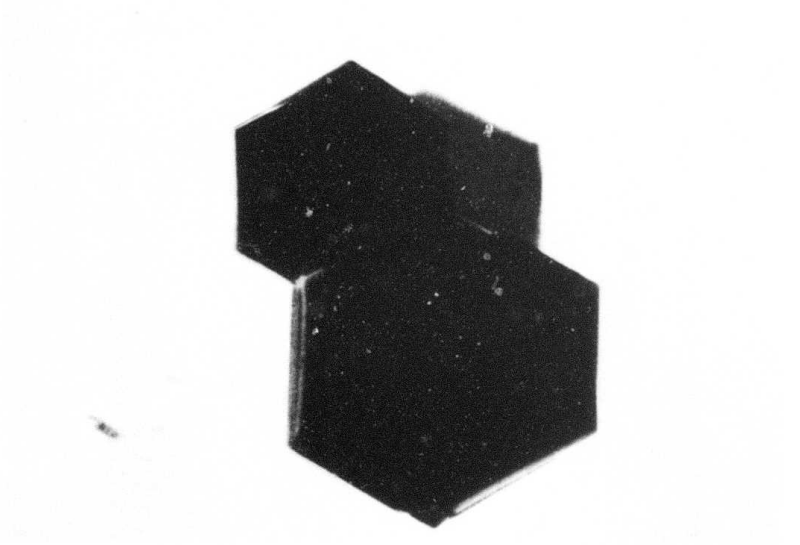

Figure 17. Cluster of Ba(Fe,Ga) Ferrite Platelets Exhibiting Stripe and Bubble Domains Lying on Top of $(Sm,Y)_3(Ga,Fe)_5O_{12}$ Epitaxial Layer Grown in $BaO-B_2O_3-BaF_2$ Solvent at an R_1 = 1.20. Polarized Transmitted Illumination (500X).

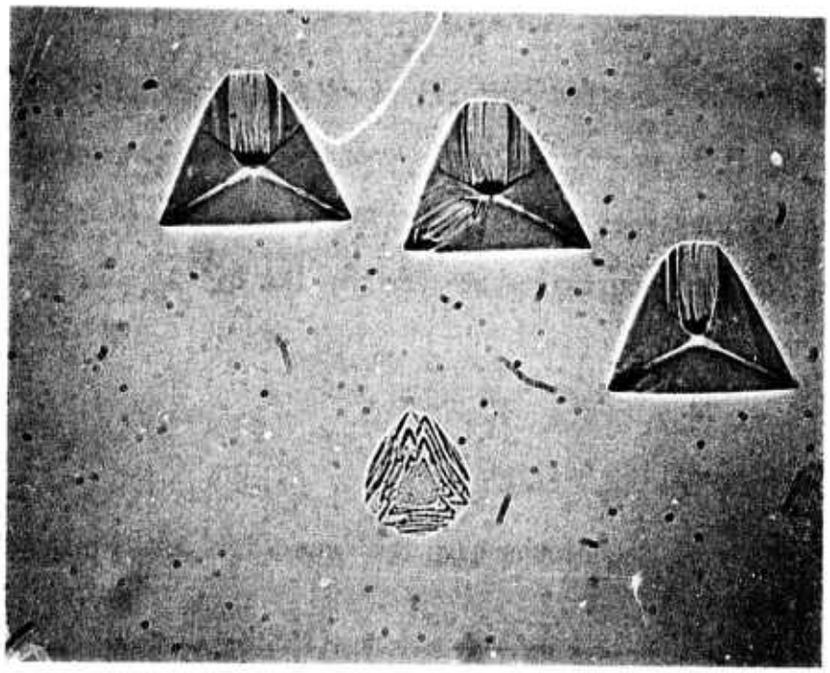

Figure 18a. Pit Morphology in $(Sm,Y)_3(Ga,Fe)_5O_{12}$ Grown in $BaO-B_2O_3-BaF_2$ Solvent at $R_1 = 1.68$. Bright Field Reflected Illumination (500X).

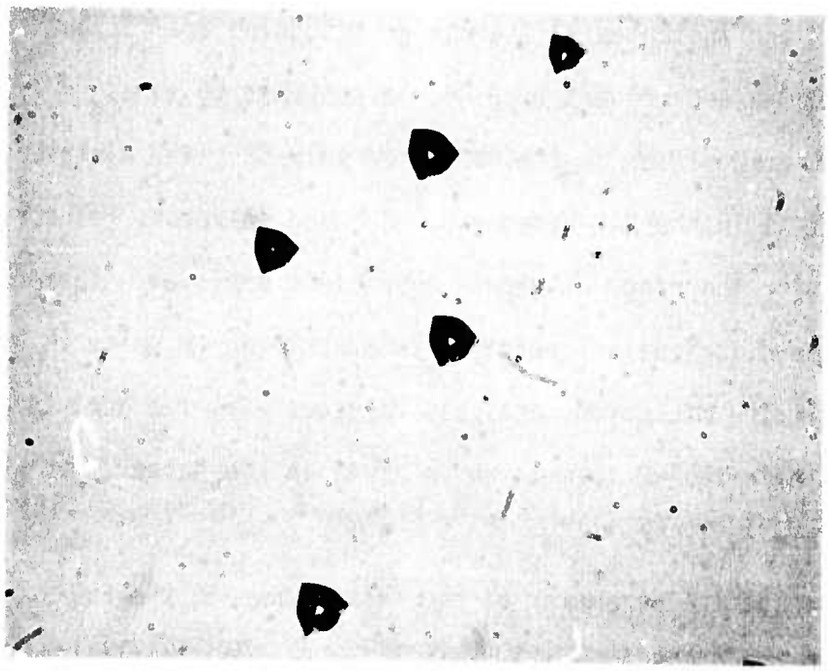

Figure 18b. Pit Morphology in $(Sm,Y)_3(Ga,Fe)_5O_{12}$ Grown in $BaO-B_2O_3-BaF_2$ Solvent at $R_1 = 0.80$. Bright Field Reflected Illumination (500X).

layer as soon after the desired temperature is reached as possible. In the $PbO-B_2O_3$ solvent, films can be routinely grown with less than five defects per cm^2 (including substrate processing defects) at an R_1 of 25 at 15°C supercooling. Similar results are achieved in the $BaO-B_2O_3-BaF_2$ solvent with an R_1 ratio of 0.80.

3.2 Film Composition Analysis

A variety of techniques have been used for determining the film composition, including the direct methods of microprobe analysis and emission spectroscopy, as well as the indirect techniques of lattice parameter and Néel temperature measurements.

The microprobe analysis was done with a modified Cambridge Stereoscan SEM and indicates an average distribution coefficient for gallium (α_{Ga}) in the BaO-based solvent of 0.84, in contrast to an α_{Ga} = 1.71 for a similar garnet composition in the PbO-based solvent. The distribution coefficient of Sm in the BaO-based and PbO-based solvents, respectively, are 0.94 and 0.73 for the range of growth conditions employed. Therefore, in both cases, the distribution coefficients are closer to unity in the BaO-based solvent. The microprobe analyses together with the Néel temperature measurements indicate 1.2 formula units of Ga in the garnet, for which the Néel temperature is 120°C.

The lattice parameter of the films grown in the $PbO-B_2O_3$ solvent at 900°C was 0.004-0.005 Å greater than films having identical Néel temperature grown in the $BaO-B_2O_3-BaF_2$ solvent at 1000°C, even though the growth rates were similar (0.7-0.8 μm/min). The films grown in the PbO-based

solvent contained 0.8-1.0 wt% Pb and 0.2-0.4 wt% Pt, both of which tend to increase the lattice parameter. Films grown in the BaO-based solution contained < 0.1 wt% Pb and Pt.

Several films were grown from the BaO-based solvent with different amounts of Sm in the solution, and the variation in lattice parameter with increasing Sm content is shown in Fig. 19.

Several thick films (35-70 μm) of both $(Sm,Y)_3(Fe,Ga)_5O_{12}$ and $Y_3Fe_5O_{12}$ were grown from the BaO-based and PbO-based solvents at constant and variable growth rates to determine any compositional variations normal to the surface of the epitaxial layer. The microprobe trace for a film of $(Sm,Y)_3(Fe,Ga)_5O_{12}$ 37.5 μm thick grown in $PbO-B_2O_3$ at a constant growth rate is shown in Fig. 20. The Pb content is very high at the substrate/epitaxial layer interface and drops off rapidly with increasing thickness until it reaches almost the background level at the surface of the film. Quantitative analysis in the first 10 μm and the last 10 μm of growth revealed a drop in Pb content from 1.1 to 0.47 wt% Pb. The variation in Ga content was within the systematic error. Another thick layer was grown in the $PbO-B_2O_3$ solution with a growth rate which was varied in seven steps from 0.28 μm/min to 0.50 μm/min as the layer grew. The resultant growth pattern is shown in Fig. 21. There are seven distinct layers revealed by etching in 160°C H_3PO_4 for 5 minutes. Very slight compositional variations are known to be sensitive to this etchant. The increasing growth rate leveled the Pb concentration in the film (within the precision of the analysis), as shown in the microprobe trace in Fig. 22, in accordance with theoretical predictions, since the distribution coefficient should go to unity as the

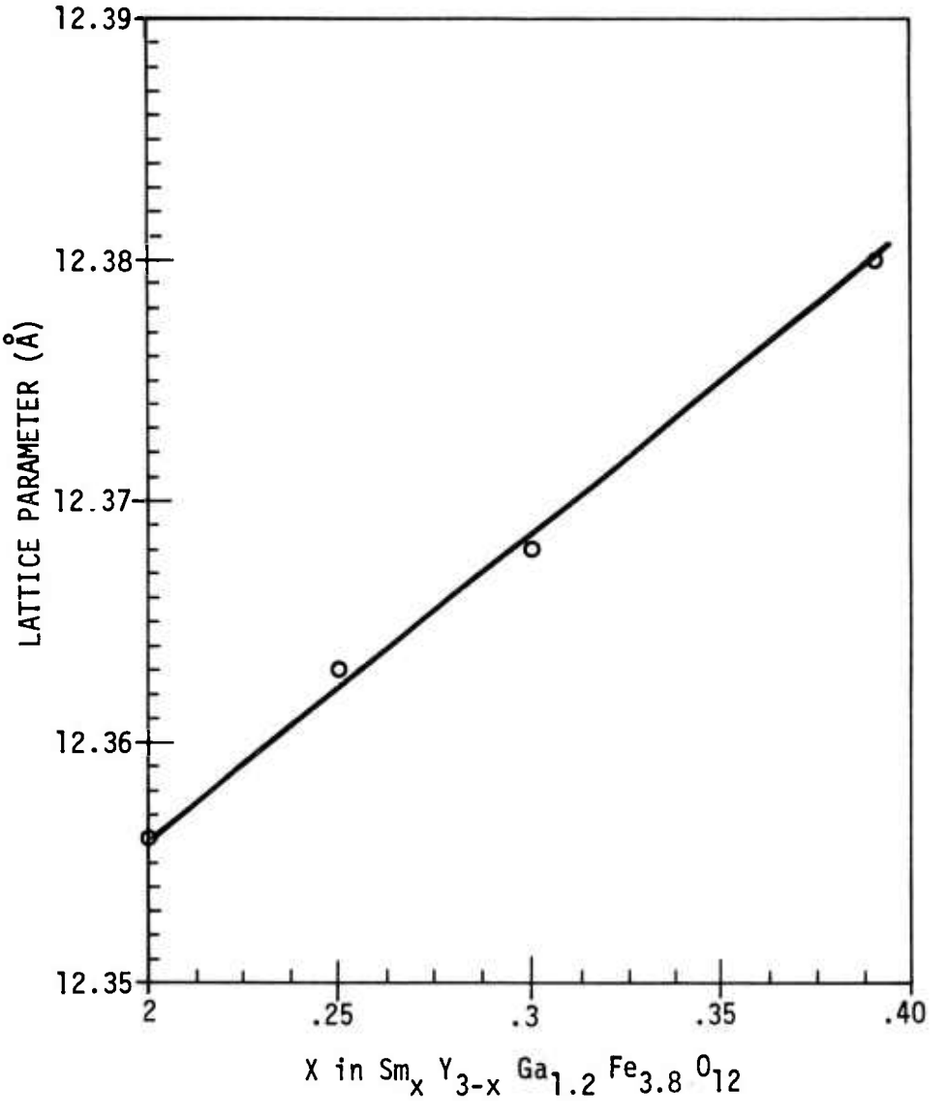

Figure 19. The Effect of Solution Sm Content on the Lattice Parameter (Measured Normal to the Substrate/Film Interface) of $(Sm,Y)_3(Ga,Fe)_5O_{12}$ Grown Epitaxially on $Gd_3Ga_5O_{12}$ in $BaO-B_2O_3-BaF_2$ Solvent at 1000°C.

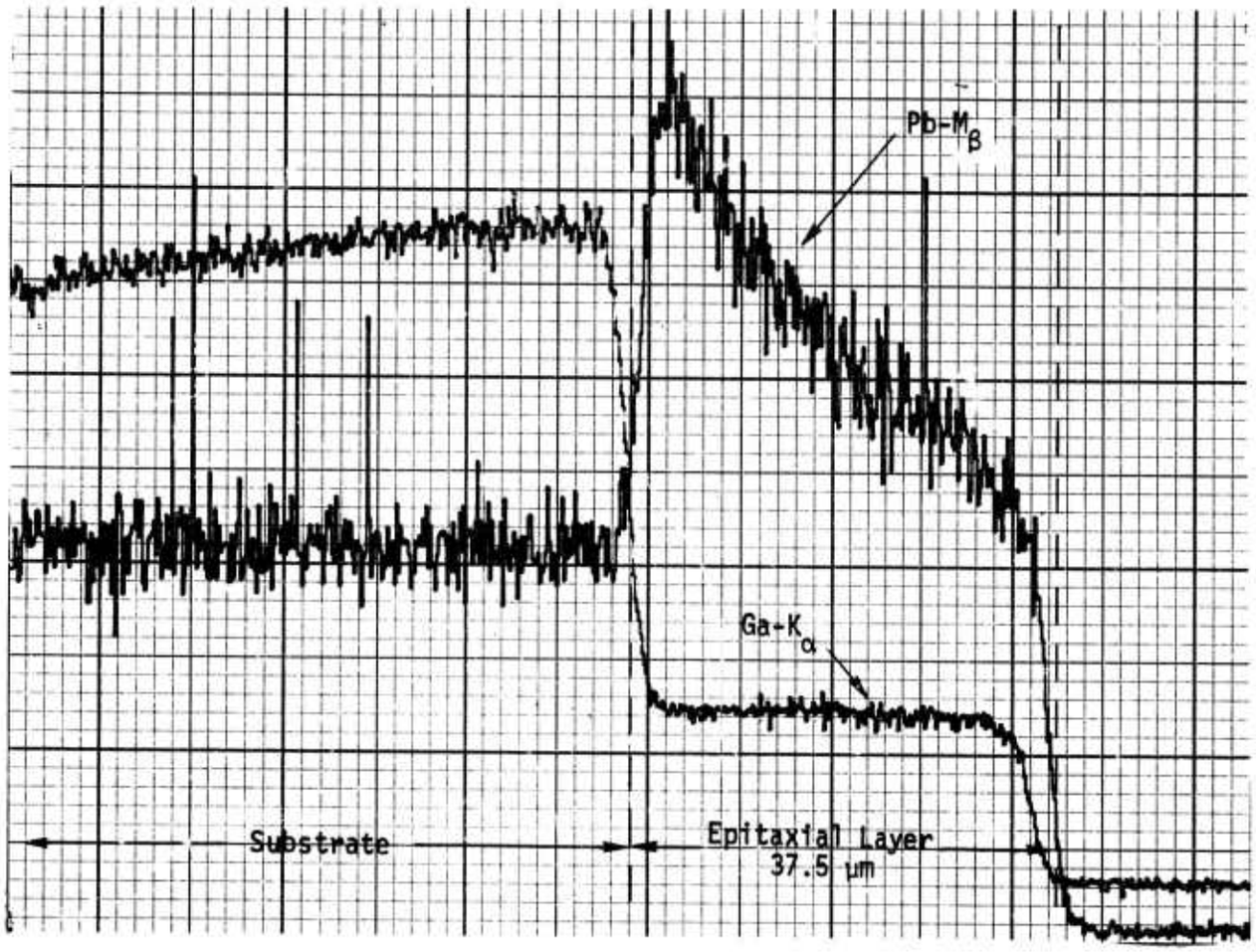

Figure 20. Microprobe Scan for Ga and Pb in $(Sm,Y)_3(Ga,Fe)_5O_{12}$ Epitaxial Layer 37.5 µm Thick. Grown in $PbO-B_2O_3$ Solvent at 900°C, 100 rpm. Growth Rate = 0.42 µm/min.

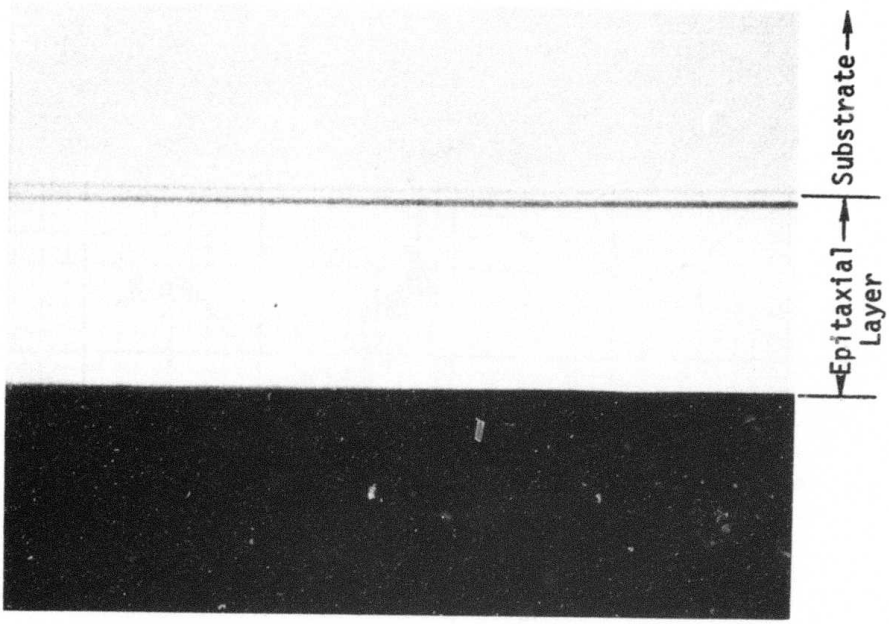

Figure 21. Growth Striations in a Fractured Section of a 55 μm Thick Layer of $(Sm,Y)_3(Ga,Fe)_5O_{12}$ Grown in $PbO-B_2O_3$ Solvent at 900°C at Seven Different Rotation Rates. Specimen was Etched in 160°C H_3PO_4 for 5 Minutes. Bright Field Reflected Illumination, 500X.

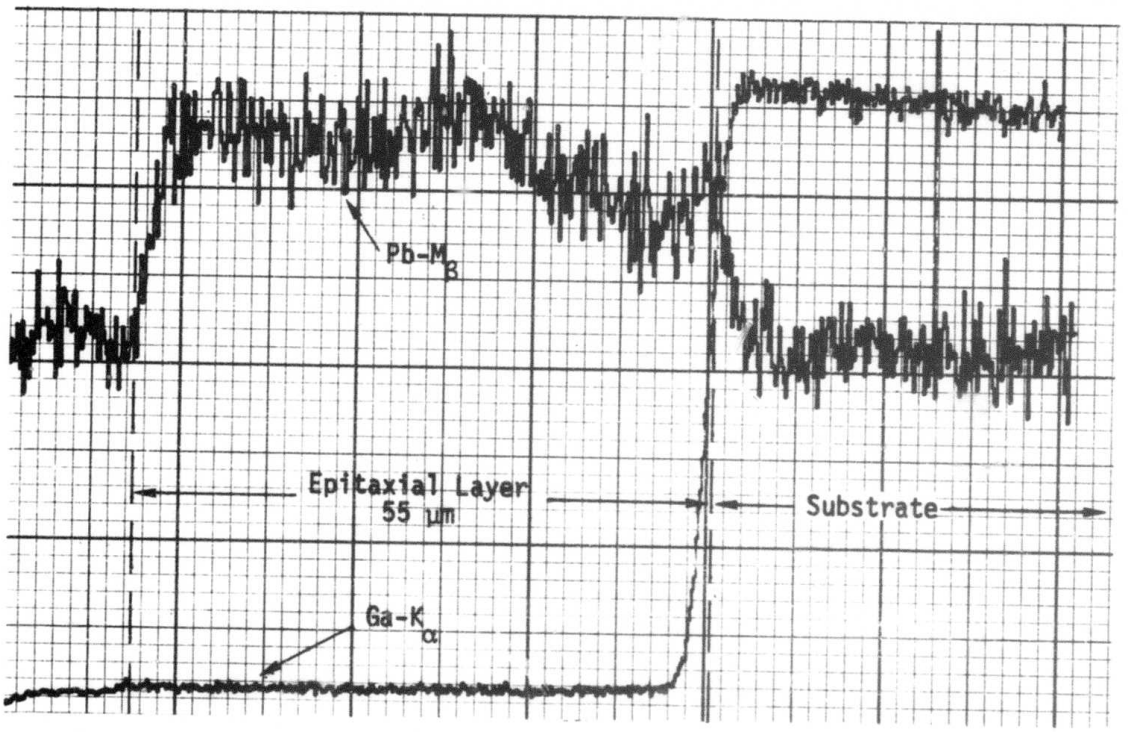

Figure 22. Microprobe Scan for Ga and Pb in the Epitaxial Layer Shown in Fig. 21.

growth rate is increased. There does not appear to be any measurable effect on the Ga concentration, however, for this range of growth rates.

A similar experiment in the BaO-based solvent was also performed. In this case, the microprobe scan for Ga was also flat, and Ba, if present, was at too low a concentration to be detected by microprobe analysis. An etch in 160°C H_3PO_4 for 5 minutes did not reveal any sign of a compositional variation. A similar scan for thick layers of $Y_3Fe_5O_{12}$ grown in BaO-based and PbO-based solvents gave identical results to those shown for $(Sm,Y)_3(Fe,Ga)_5O_{12}$.

3.3 Optical Properties of the Garnet Films

Earlier optical absorption measurements of $(Gd,Y,Yb)_3(Ga,Fe)_5O_{12}$ epitaxial layers of similar composition grown in the BaO-based and PbO-based solvents indicated significant differences in absorption, which were assumed to be related to the different amounts of impurities in the films. A more detailed study has been completed during this contract period using $Y_3Fe_5O_{12}$ as the vehicle to ensure an invariant garnet composition for films grown in each solvent.

The measurements were performed on a double beam spectrophotometer, and I/I_o was measured using a circular aperture 3.97 mm in diameter. The absorption coefficient α was calculated from the single layer formula

$$I/I_o = \frac{(1 - R)^2 \exp(-\alpha t)}{1 - R^2 \exp(-2\alpha t)} \quad , \qquad (1)$$

where I = the intensity of light transmitted through the sample,

R = the reflectivity,

t = the thickness of the epitaxial layer, and

α = the absorption coefficient of the epitaxial layer.

The reflectivity was measured to be 0.136 in the wavelength region 2-2.5 μm where the absorption for the garnets is negligible. This value was assumed constant for the entire wavelength region of interest, and was assumed to be the same for garnets grown in the PbO-based solvent and the BaO-based solvent. For some of the measurements, the epitaxial layer was lapped off one side of the substrate, and for the rest of the measurements, the entire substrate was lapped off as well to evaluate possible contributions to the absorption from the substrate/epitaxial layer interface.

The absorption spectra were measured for films of $Y_3Fe_5O_{12}$ grown at different growth rates in the PbO-B_2O_3 solvent at 900, 950 and 1000°C, and in the BaO-B_2O_3 solvent at 1000°C. The results are shown in Fig. 23. Curve D was measured on a thick film (∿50 μm) with the substrate attached. Subsequently, the substrate was lapped off and the resulting spectrum was identical to that with the substrate attached. Hence, it was concluded that the measurement of the absorption coefficient was insensitive to the presence or absence of the $Gd_3Ga_5O_{12}$ substrate. Similarly, films of different thickness ranging from 5-50 μm, grown at identical growth rate and temperature yielded the same optical absorption spectrum within experimental error.

The results in Fig. 23 indicate that the absorption coefficient (1) increases with increasing growth rate, (2) decreases with increasing growth temperature at comparable growth rates, and (3) is much less for films grown in the BaO-based solvent than in the PbO-based solvent. The highest optical absorption coefficient (Curve A, Fig. 23) was observed for

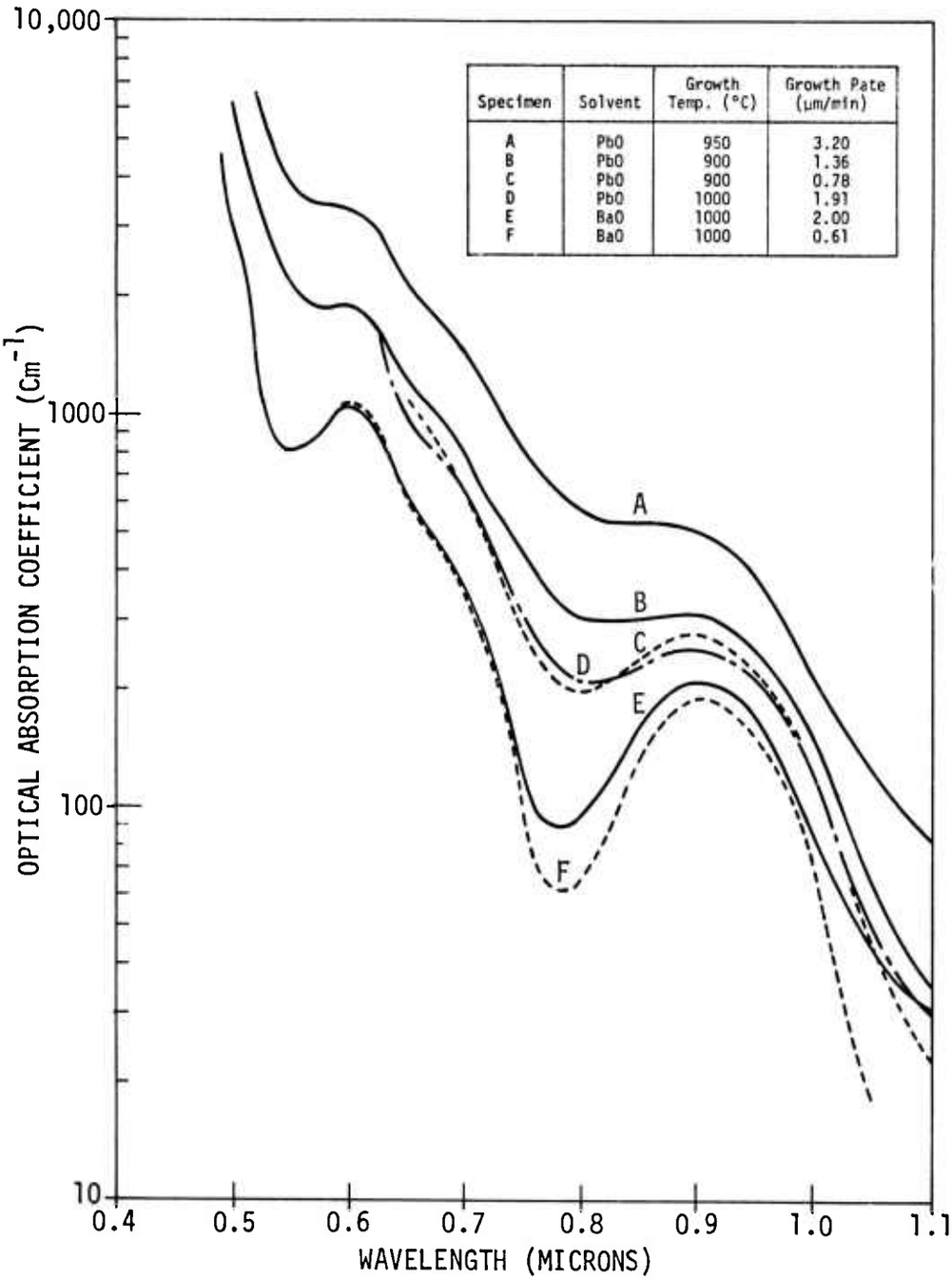

Figure 23. Optical Absorption Curves for $Y_3Fe_5O_{12}$ Grown in PbO-Based and BaO-Based Solvents.

a film grown in $PbO-B_2O_3$ at an intermediate temperature (950°C), but it had a very high growth rate of 3.2 μm/min. These data are consistent with an increase in solvent incorporation with increasing growth rate and decreasing temperature, which leads to the formation of Fe^{2+} or Fe^{4+}[22]. Emission spectrographic analysis of the films of Curves C and D after the substrates were lapped off indicated 0.6 wt% Pb in both films, which is consistent with the spectra obtained. The lattice parameters of the films ranged from 12.382 Å for A to 12.370 Å for C and D to 12.368 Å for F, again consistent with a decrease in solvent impurity content.

3.4 Magnetic Properties of the Garnet Films

Magnetic characterization of the garnet epitaxial layers is essential to their evaluation for magnetic bubble devices. The film properties that were measured and the measurement techniques are given in Table VII. The details of these techniques have been fully discussed in earlier reports, and here we shall discuss some of the results for $(Sm,Y)_3(Fe,Ga)_5O_{12}$.

The variation of the magnetic properties with growth rate and with growth temperature is shown in Table VIII for garnet films grown in the BaO-based and PbO-based solvents. The magnetization increases with increasing growth rate in the BaO-based solvent, although the Néel temperature and lattice temperature change only slightly, which indicates very little difference in Ga content for films grown at growth rates ranging from 0.05-1.28 μm/min. The increase in magnetization, which produces a corresponding decrease in the characteristic length, can be rationalized on the basis of

TABLE VIII

Magnetic Properties of $(Sm,Y)_3(Ga,Fe)_5O_{12}$

Solvent	Temp. (°C)	Growth Rate (μm/min)	h (μm)	ℓ (μm)	4πM (Gauss)	H_{col} (Oe)	H_c (Oe)	T_N (°C)	Lattice* Parameter (Å)
$BaO-B_2O_3-BaF_2$	1000	0.05	3.0	1.27	107	20.9	0.46	119.8	12.363
"	1000	0.26	3.9	1.36	93	22.7	0.70	115.3	12.362
"	1000	0.51	4.1	1.19	-	30.6	0.80	116.4	12.363
"	1000	0.68	6.8	1.01	113	51.3	0.40	120.0	12.364
"	1000	1.16	5.8	0.82	117	54.8	0.29	117.0	12.365
"	1000	1.28	5.1	0.71	149	70.0	0.24	118.0	12.366
"	1021	0.34	10.1	1.36	85	40.3	0.34	113.4	12.358
"	1010	0.73	7.3	0.98	104	50.0	0.39	115.6	12.363
"	1000	0.99	4.7	0.77	121	52.3	1.40	116.6	12.364
"	990	1.3	3.9	0.71	141	57.4	0.34	118.4	-
"	981	1.6	3.9	0.50	151	73.8	0.29	119.7	12.368
"	972	1.6	3.2	0.43	180	86.0	0.26	121.6	-
"	960	1.3	3.8	0.40	208	111.0	0.32	122.3	12.376
$PbO-B_2O_3$	900	0.13	2.8	0.82	-	11.6	1.30	117.2	12.366
"	900	0.22	3.6	0.87	162	53.8	0.33	120.2	12.369
"	900	0.42	2.4	0.79	124	31.7	0.62	121.1	12.382
"	900	0.50	2.0	0.85	110	22.0	-	121.0	12.371
"	900	0.38	3.0	>1.00	-	18.2	0.71	116.8	-
"	930	0.29	8.6	2.34	76	23.0	0.39	116.9	12.365
"	920	0.43	6.4	1.15	101	41.4	0.39	119.0	-
"	910	0.54	5.4	0.92	124	52.5	0.32	120.2	12.370
"	900	0.79	7.9	0.54	155	95.4	0.17	122.8	12.382
"	890	0.76	3.8	0.56	156	71.2	0.34	123.7	12.382
"	880	0.87	2.6	0.55	168	62.0	0.43	124.4	-
"	870	0.85	1.7	0.50	-	-	0.64	125.1	12.382

* Normalized to substrate lattice parameter = 12.382Å, measured perpendicular to substrate/epitaxial layer interface. h = thickness, ℓ = characteristic length, 4πM = saturation magnetization, H_{col} = collapse field, H_c = coercive force, T_N = Néel temperature.

a change in the relative distribution coefficient of Ga between dodecahedral and tetrahedral sites, as discussed in Ref. (14). Any difference in the total Ga distribution coefficient with growth rate would be expected to lower the Néel temperature, since the distribution coefficient should go to unity as the growth rate is increased. There is a more pronounced change in the Néel temperature, and hence Ga content, with growth temperature for films grown in either solvent, as shown in Fig. 24. The growth rate increased as the growth temperature decreased, so this plot displays a combination of the growth rate and temperature effect upon the Ga distribution coefficient. The Ga content increases by $\sim$0.0072 formula units for every 1°C decrease in the Néel temperature, and therefore, decreases by $\sim$0.001 formula unit for every 1°C supercooling for both the PbO-based and BaO-based solvents. The lattice parameter was larger for films of comparable Néel temperature grown in the PbO-based solvent compared to those grown in the BaO-based solvent, which tends to decrease the amount of stress induced anisotropy with a resultant change in characteristic length.

The Sm^{3+} ion has a large damping factor and greatly reduces the domain wall mobility of the $(Sm,Y)_3(Ga,Fe)_5O_{12}$ garnet. The effect of Sm content upon the mobility is shown in Fig. 25 for a series of films grown in the BaO-based solvent. It is apparent that as little Sm as possible is desirable for increased domain wall mobility. However, below 0.2 formula units of Sm, the lattice mismatch becomes great enough (> 0.015 Å) to induce cracking in the films. From this viewpoint, it would be desirable to grow films in the PbO-based solvent at low temperatures and high growth rates to induce the largest amount of Pb possible in the film.

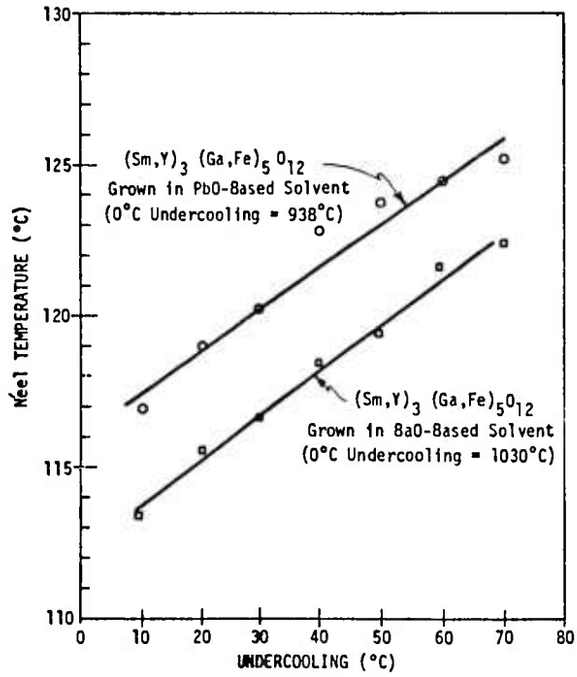

Figure 24. Variation of Néel Temperature with Supercooling for $(Sm,Y)_3(Ga,Fe)_5O_{12}$ Grown in $PbO-B_2O_3$ and $BaO-B_2O_3-BaF_2$ Solvent.

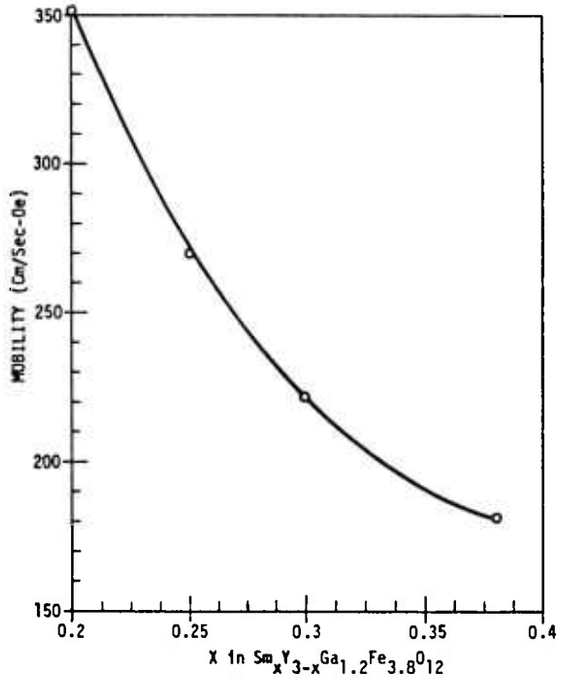

Figure 25. Variation of Domain Wall Mobility with Solution Sm Content for $(Sm,Y)_3Ga_{1.2}Fe_{3.8}O_{12}$ Grown in $BaO-B_2O_3-BaF_2$ Solvent at 1000°C.

The temperature dependence of the characteristic length, wall energy and magnetization is shown for $Sm_{.38}Y_{2.62}Ga_{1.2}Fe_{3.8}O_{12}$ grown in the BaO-based solvent in Fig. 26. The temperature dependence of collapse field for several films of different composition (including a $(Eu,Y)_3(Ga,Fe)_5O_{12}$ composition for comparison) grown in each of the solvents is shown in Fig. 27. It can be seen that as the Ga content increases from 1.0→1.1→1.2 formula units, a maximum develops in the H_{col} versus temperature curves, which shifts to higher temperatures as the Ga is increased. It is desirable to adjust the composition so that the collapse field matches the temperature dependence of the bias field.

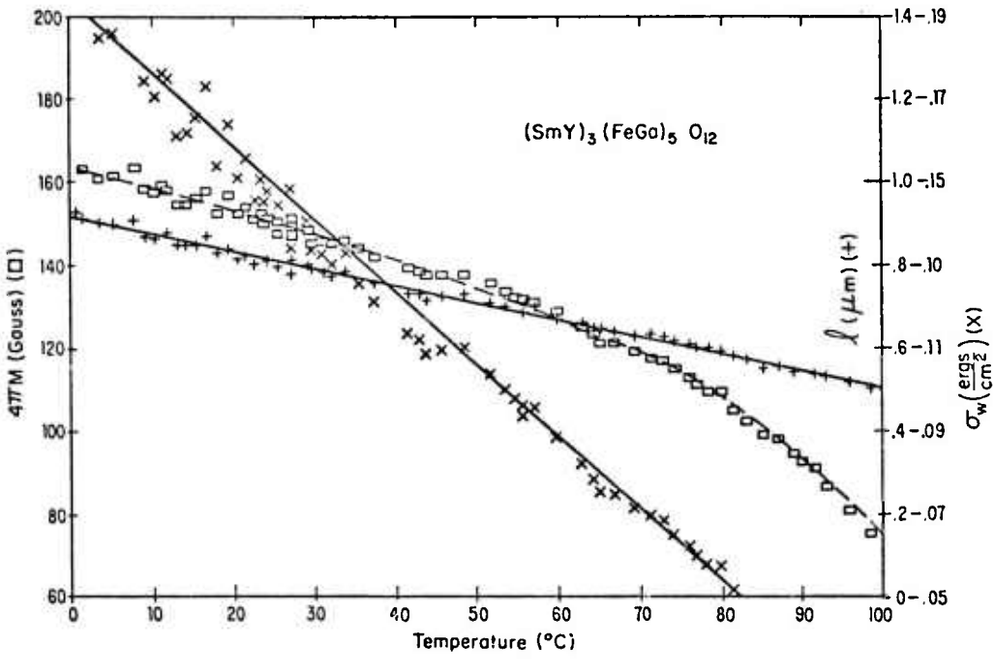

Figure 26. Temperature Coefficients of Characteristic Length ℓ, Magnetization $4\pi M$ and Wall Energy σ_w for $(Sm,Y)_3(Ga,Fe)_5O_{12}$.

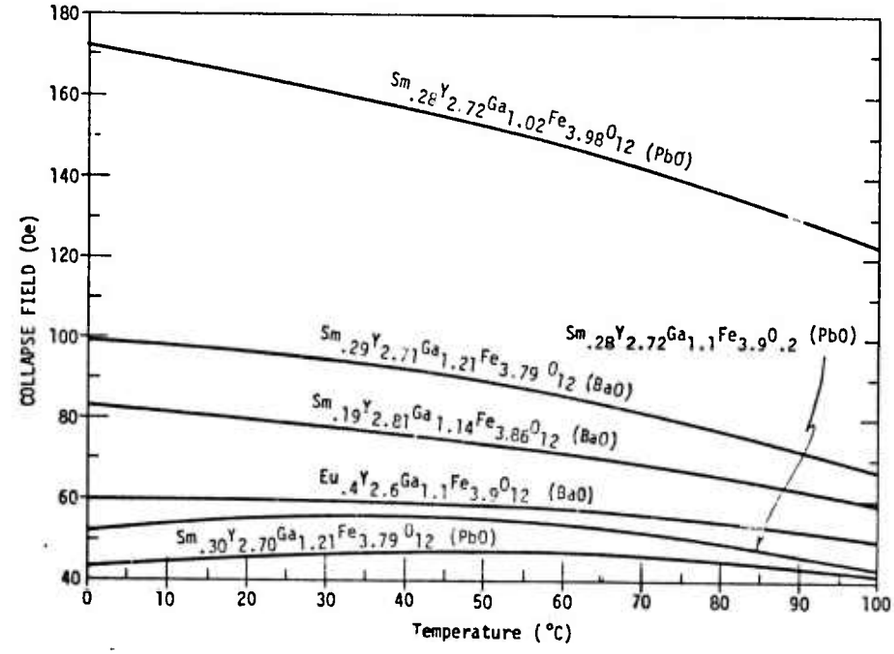

Figure 27. Temperature Dependence of the Collapse Field for Various Garnet Compositions Grown in $PbO-B_2O_3$ and $BaO-B_2O_3-BaF_2$ Solvents. The Compositions Shown Were Determined by Microprobe Analysis.

SECTION IV

4.0 CONCLUSIONS

1. Controlled and reproducible growth of the temperature stable garnet $(Sm,Y)_3(Fe,Ga)_5O_{12}$ has been demonstrated in both the $BaO-B_2O_3-BaF_2$ solvent and the $PbO-B_2O_3$ solvent using a horizontally rotating substrate with the liquid phase epitaxial dipping technique.

2. The reproducibility of the process is considerably better with the BaO-based solvent since it is relatively non-volatile and the saturation temperature stays relatively constant from run to run. However, reproducibility can be achieved in the PbO-based solvent by programming the growth temperature and time from run to run.

3. The magnetic properties of garnet epitaxial layers grown from either solvent are quite similar. The major differences arise from the differences in lattice mismatch between films and substrate due to the different amount of Pb and Ba impurities, which results in a different amount of stress induced anisotropy for films having the same rare earth and Ga content. The larger amount of Pb present in PbO-grown films also increases the optical absorption coefficient for these films, which may have implications for magneto-optic applications.

4. Defect densities and thickness uniformities of the films grown in each solvent are comparable, and can be kept below $5/cm^2$ on a routine basis. A higher rotation rate is needed to provide good thickness uniformity in the BaO-based solvent, but this provides little experimental difficulty.

5. Since the BaO-based solvent is much less volatile and the

properties of films grown in this solvent are comparable to those produced by growth in the PbO-based solvent, it is superior to the $PbO-B_2O_3$ solvent for the LPE growth of the bubble garnets.

The $(Sm,Y)_3(Ga,Fe)_5O_{12}$ composition which has been developed during this last contract period appears to offer a reasonable compromise between high data rate and temperature stability for use in magnetic bubble memory devices.

REFERENCES

1. H. J. Van Hook, J. Amer. Ceram. Soc. 44, 213 (1961).

2. R. C. Linares, J. Amer. Ceram. Soc. 45, 307 (1962).

3. A. H. Bobeck, E. G. Spencer, L. G. Van Uitert, S. C. Abrahams, R. L. Barns, W. H. Grodkiewicz, R. C. Sherwood, P. H. Schmidt, D. H. Smith and E. M. Walters, Appl. Phys. Lett. 17, 131 (1970).

4. R. Hiskes, T. L. Felmlee and R. A. Burmeister, J. Electron. Mater. 1, 458 (1972).

5. L. K. Shick and J. W. Nielsen, J. Appl. Phys. 42, 1554 (1971).

6. F. C. Rossol, Phys. Rev. Lett. 24, 1021 (1970).

7. R. Hiskes and R. A. Burmeister, AIP Conf. Proc., No. 10, Part 1, 304 (1972).

8. A. H. Bobeck, Bell Syst. Tech. J. 46, 1901 (1967).

9. L. G. Van Uitert, D. H. Smith, W. A. Bonner, W. H. Grodkiewicz, and G. J. Zydzik, Mater. Res. Bull. 5, 455 (1970).

10. P. C. Michaelis, 1973 INTERMAG Conf., Washington, D.C., April 1973.

11. P. Chaudari, J. J. Cuomo and R. J. Gambino, IBM J. Res. Develop. 17, 66 (1973).

12. D. M. Heinz, P. J. Besser, J. M. Owens, J. E. Mee and G. R. Pulliam, J. Appl. Phys. 42, 1243 (1971).

13. A. J. Kurtzig and M. Dixon, J. Appl. Phys. 43, 2883 (1972).

14. R. Hiskes, Semiannual Technical Report, Magnetic Rare Earth Compounds III, ARPA Contract No. DAAH01-72-C-0996, January 1973.

15. E. A. Giess, J. D. Kuptsis and E. A. D. White, J. Cryst. Growth 16, 36 (1972).

16. J. A. Burton, R C. Prim and W. P. Slichter, J. Chem. Phys. 21, 1987 (1953).

17. E. A. D. White and J. D. C. Wood, J. Crystal Growth 17, 315 (1972).

18. R. G. Warren, J. E. Mee, R. D. Henry, F. S. Stearns, and B. C. Whitcomb, Quarterly Technical Report, Thin Film Garnet Manufacturing Method, Air Force Materials Laboratory Contract No. F33615-72-C-1299, May 1973.

19. C. D. Brandle, D. C. Miller and J. W. Nielsen, J. Cryst. Growth 12, 195 (1972).

20. R. Hiskes, T. L. Felmlee and R. A. Burmeister, Semiannual Technical Report, Magnetic Rare Earth Compounds, ARPA Contract No. DAAH01-70-C-1106, December 1970.

21. R. Hiskes, T. L. Felmlee and R. A. Burmeister, Final Technical Report, Magnetic Rare Earth Compounds, ARPA Contract No. DAAH01-70-C-1106, June 1971.

22. R. Hiskes and R. A. Burmeister, Final Technical Report, Magnetic Rare Earth Compounds II, ARPA Contract No. DAAH01-71-C-1259, June 1972.

23. S. L. Blank and J. W. Nielsen, J. Cryst. Growth 17, 302 (1972).

24. L. Shartsis and H. F. Shermer, J. Amer. Ceram. Soc. 37, 544 (1954).

25. R. Ghez and E. A. Giess, Mater. Res. Bull. 8, 31 (1973).

26. D. C. Miller, J. Electrochem. Soc. 120, 678 (1973).